iScience

CellPress
OPEN ACCESS

Article

Mof plays distinct roles in hepatic lipid metabolism under healthy or non-alcoholic fatty liver conditions

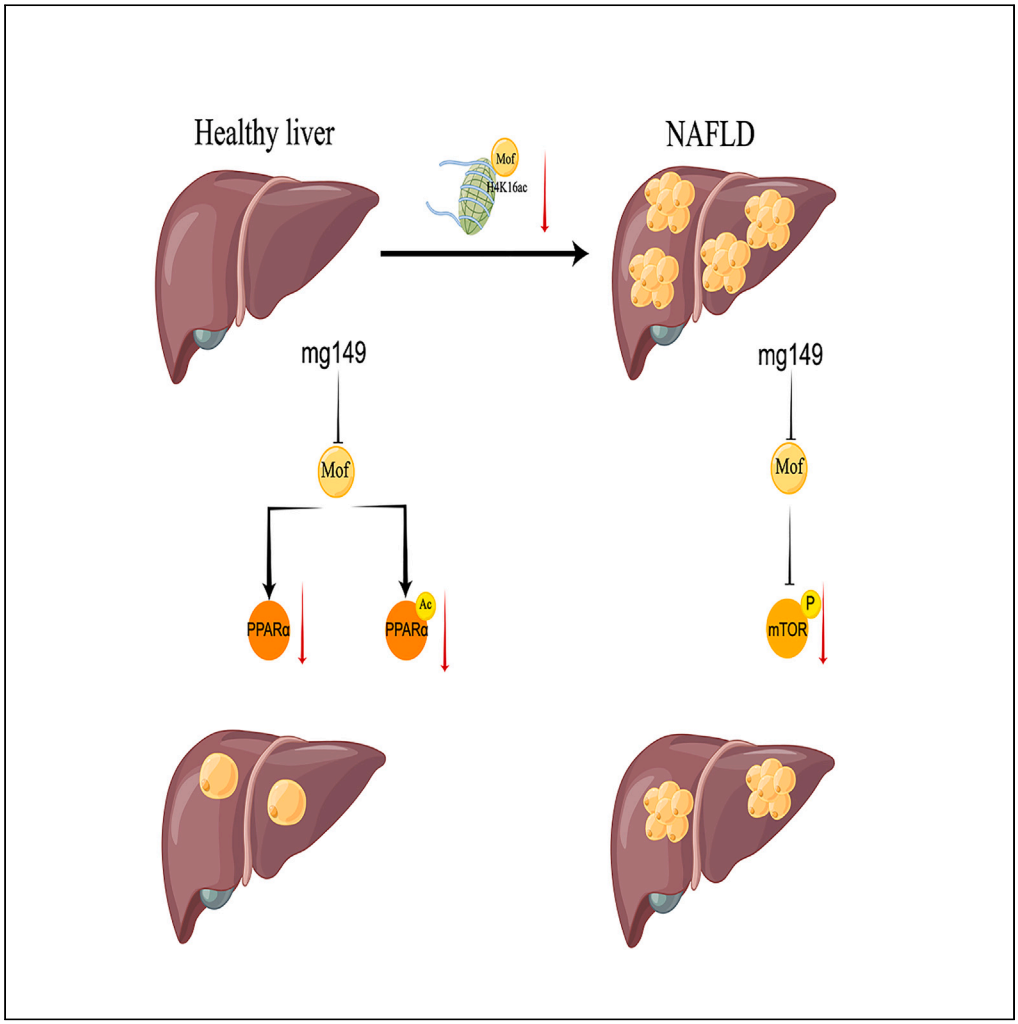

Xinghong Guo, Kai Liang, Longqing Xia, ..., Xiangzhi Li, Xinguo Hou, Li Chen

houxinguo@sdu.edu.cn (X.H.)
chenli3@email.sdu.edu.cn (L.C.)

Highlights

Mof is important for hepatic lipid metabolism

Mof regulates lipid metabolism via PPARα under healthy condition

Mof regulates lipid metabolism via the mTOR under NAFLD condition

Mof inhibition ameliorates hepatic lipid metabolism disorder in DIO mice

Guo et al., iScience 26, 108446
December 15, 2023
https://doi.org/10.1016/j.isci.2023.108446

iScience

CellPress
OPEN ACCESS

Article

Mof plays distinct roles in hepatic lipid metabolism under healthy or non-alcoholic fatty liver conditions

Xinghong Guo,[1,3,4,5,6] Kai Liang,[1,3,4,5,6] Longqing Xia,[1] Xu Zhang,[2] Jinbo Liu,[1,3,4,5] Chuan Wang,[1,3,4,5] Jinquan Li,[1,3,4,5] Xiangzhi Li,[2] Xinguo Hou,[1,3,4,5,*] and Li Chen[1,3,4,5,7,*]

SUMMARY

The disturbance of hepatic lipid metabolism has a strong association with non-alcoholic fatty liver disease (NAFLD) and diabetes. Mof, an acetyltransferase involved in obesity and carbon metabolism, has not been thoroughly examined in its connection to hepatic metabolism. We aimed to explore the impact of Mof on hepatic lipid metabolism. The alteration of Mof expression was found in both obese mice and NAFLD human liver. The genes regulated by Mof were closely associated with lipid metabolism. In normal mice or hepatic cells, the down-regulation or inhibition of Mof resulted in increased lipid accumulation due to decreased PPARα expression. Conversely, in diet-induced obesity (DIO) mice or hepatic cells treated with palmitic acid, the inhibition of Mof led to improved lipid metabolism, attributed to the reduction in *p*-mTOR/mTOR levels. In summary, Mof exhibited distinct roles in lipid metabolism under different conditions. The inhibition of Mof may hold potential as a therapeutic target for hepatic lipid metabolism disturbances.

INTRODUCTION

The liver plays a crucial role in the metabolism of carbohydrates, lipids, and amino acids within the body. Disruptions in hepatic metabolism have been closely linked to conditions such as obesity, non-alcoholic fatty liver disease (NAFLD), and type 2 diabetes mellitus (T2DM). The consumption of a high-fat diet has been shown to promote the development of obesity and the accumulation of lipids within the liver, leading to changes in glucose, lipid, and amino acid levels, as well as hepatocellular energy levels.[1] Such alterations compose the key pathophysiological features of metabolic disease. For example, the elevation of intra-hepatic triglyceride (TG) is the hallmark of NAFLD.[2] The acceleration of insulin resistance and glucogenesis, which are key features of T2DM, is facilitated by an increase in hepatic TG deposition.[3] Furthermore, the disruption of hepatic lipid metabolism hinders the urea cycle, resulting in elevated levels of serum amino acids, particularly alanine.[4] The heightened amino acid levels activate the mTOR signaling pathway and stimulate the secretion of glucagon. This hormone binds to the glucagon receptor in the liver, promoting glucogenesis and establishing the "liver-α cells" axis.[5,6] Consequently, rectifying hepatic lipid metabolism, especially TG accumulation is crucial in halting the progression of NAFLD and T2DM.

Considerable efforts have been dedicated to investigating hepatic lipid metabolism and improving NAFLD through the identification of PPARα agonists and the inhibition of mammalian target of rapamycin complex 1 (mTORC1) as potential therapeutic targets.[7–9] PPARα, a ligand-activated nuclear receptor highly expressed in the liver, functions as a nutritional sensor responsible for modulating rates of lipogenesis, fatty acid oxidation, and ketone body synthesis during periods of feeding and starvation.[10] Acting as a transcription factor, PPARα primarily regulates genes involved in β-oxidation, glucose production, and fatty acid transport.[11] The deletion of hepatocyte PPARα hampers the breakdown of fatty acids, leading to the accumulation of lipids and the development of liver steatosis. The administration of potent PPARα agonists effectively reverses the buildup of lipids, inflammation, and fibrosis in individuals consuming high-fat diets.[8] The mTOR signaling pathway has been extensively studied for its involvement in obesity, NAFLD, and T2DM. mTORC1, a component of the mTOR pathway, plays a crucial role in lipid metabolism by promoting lipogenesis and inhibiting lipophagy.[12] Inhibiting mTORC1 in hepatocytes reduces insulin-induced fat synthesis, suggesting that targeting mTORC1 inhibition may be a viable target for hepatic lipid dysregulation.[13] Selective inhibition of mTORC1 *in vivo* has been found to enhance fatty acid oxidation, promote lysosomal biogenesis, and suppress *de novo* lipogenesis, leading to improved hepatic metabolism. This discovery suggests that targeting mTORC1 could be a potential therapeutic approach for NAFLD.[9]

[1]Department of Endocrinology, Qilu Hospital of Shandong University, Jinan, Shandong 250012, China
[2]Shandong Provincial Key Laboratory of Animal Cells and Developmental Biology, Life Science School of Shandong University, Qingdao, Shandong 266237, China
[3]Institute of Endocrine and Metabolic Diseases of Shandong University, Jinan, Shandong 250012, China
[4]Key Laboratory of Endocrine and Metabolic Diseases, Shandong Province Medicine & Health, Jinan, Shandong 250012, China
[5]Jinan Clinical Research Center for Endocrine and Metabolic Disease, Jinan, Shandong 250012, China
[6]These authors contributed equally
[7]Lead contact
*Correspondence: houxinguo@sdu.edu.cn (X.H.), chenli3@email.sdu.edu.cn (L.C.)
https://doi.org/10.1016/j.isci.2023.108446

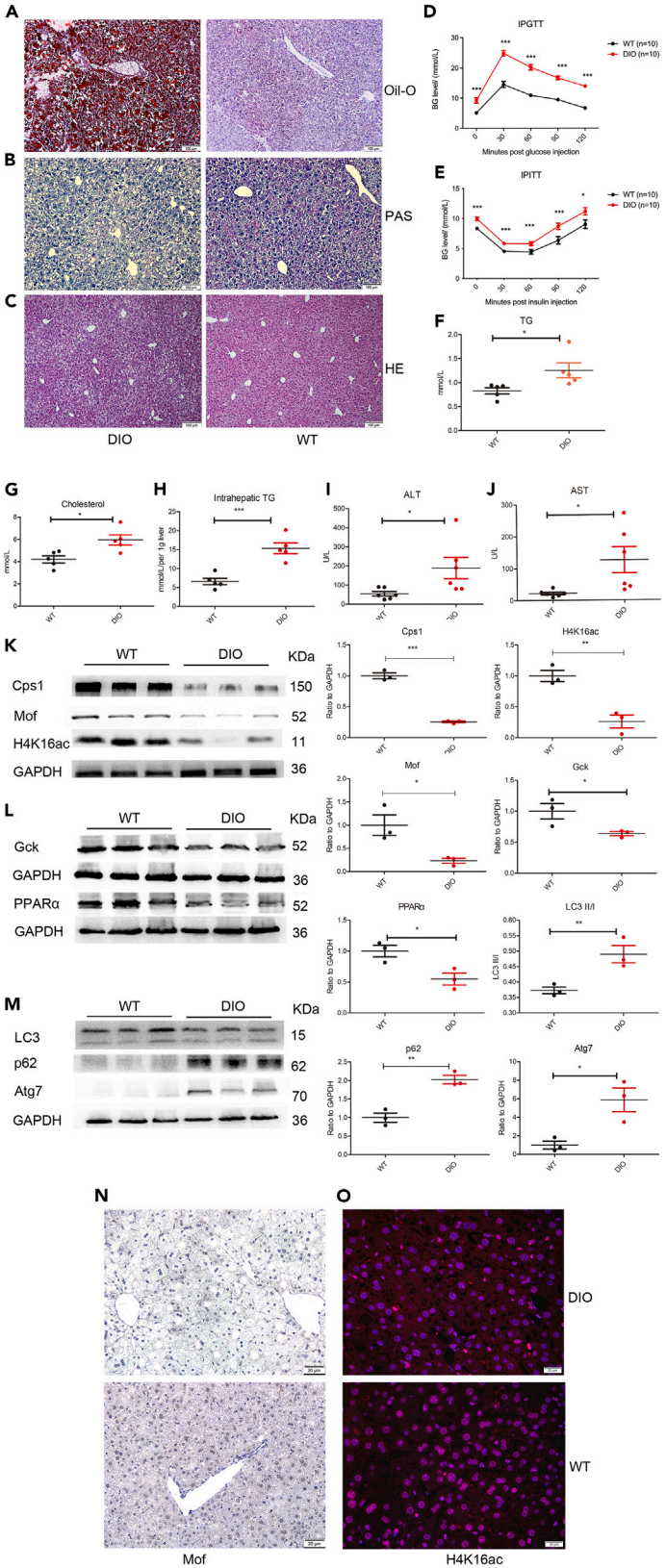
A
B
C
Oil-O
PAS
HE
DIO
WT
D
IPGTT
WT (n=10)
DIO (n=10)
BG level (mmol/L)
Minutes post glucose injection
E
IPITT
Minutes post insulin injection
F
TG
mmol/L
G
Cholesterol
H
Intrahepatic TG
I
ALT
J
AST
K
Cps1
Mof
H4K16ac
GAPDH
KDa
150
52
11
36
Ratio to GAPDH
L
Gck
PPARα
M
LC3
p62
Atg7
15
62
70
N
O
Mof
H4K16ac

Figure 1. Mof and H4K16ac expressions were down-regulated in DIO livers

(A–C) The livers of WT and DIO mice were subjected to Oil-O, PAS, and HE staining. Scale bar: 100 μm. See also Figure S4A.

(D and E) Impaired glucose and insulin tolerance in DIO mice were demonstrated through IPGTT and IPITT (n = 10).

(F–H) Disturbance in lipid metabolism was indicated by measurements of serum TG, cholesterol, and intra-hepatic TG (n = 5).

(I and J) Hepatic damage was reflected by levels of ALT and AST (n = 6).

(K–M) Decreased Mof and H4K16ac levels, as well as impaired amino acid, glucose, lipid metabolism, and autophagy, were observed through western blotting (n = 3). GAPDH was the loading control, with quantification in the right panel.

(N) Decreased Mof expression in DIO mice were demonstrated through IHC staining. Scale bar: 20 μm.

(O) Reduced H4K16ac level in DIO mice were demonstrated through IF staining. Scale bar: 20 μm.

Graph data were presented as mean ± SEM. In D–J, n represents the number of mouse. In K–M, n represents the number of western blotting data. *$p < 0.05$, **$p < 0.01$, ***$p < 0.001$ (Student's *t* test).

Male absent on the first (Mof), also known as lysine acetyltransferase 8 (Kat8), is a highly conserved acetyltransferase that plays a crucial role in promoting histone 4 lysine 16 acetylation (H4K16ac).[14] It is situated at a critical intersection of various biological processes, including oncogenesis, DNA damage response, cellular proliferation, and stem cell development.[15] The interaction between Mof and Sirt1-mediated H4K16ac is a key histone modification that influences the outcome of autophagy.[16] Additionally, Mof has the ability to acetylate non-histone proteins such as IRF3, p53, and Nrf2.[17–19] Recently, Mof has garnered significant attention in the field of metabolism. It has been observed that Mof is conserved as an obesity-related gene across various species, ranging from *C.elegans* to human beings.[20,21] Mof serves as a positive regulator for transcription and respiration in mitochondria, hereby playing crucial roles in oxidative phosphorylation.[22] In the context of lipid metabolism, studies on Mof congenital knockdown mice have demonstrated a decline in insulin sensitivity and resistance to diet-induced obesity.[23] This can be attributed to the absence of Glut2 in adipose tissues, which is mediated through the Mof-PPARγ signaling pathway. Furthermore, additional research has indicated that Mof knockdown in embryonic stem cells or neurons leads to a reduction in fatty acid oxidation and enhanced lipid accumulation.[24,25] Thus, it is plausible that Mof plays a crucial role in the regulation of lipid metabolism, albeit with potential variations in its ultimate effects under different circumstances.

Our previous findings indicated that the suppression of Mof expression resulted in reduced blood glucose levels, exacerbated insulin resistance, and diminished α cell mass and glucagon secretion.[26] Notably, the administration of mg149, an inhibitor of Mof acetyltransferase, exhibited a positive impact on glucose levels in mice with diet-induced obesity.[27] Additionally, there have been indications suggesting the involvement of Mof in hepatic lipid accumulation.[28] Nevertheless, the precise contribution of Mof to hepatic lipid metabolism remains undisclosed. Consequently, the present study aims to elucidate the impact of Mof on this metabolic process. Our study revealed that Mof exhibited diverse functions in hepatic metabolism in various conditions. Specifically, under normal physiological conditions, the knockdown or inhibition of Mof resulted in an elevation in hepatic TG accumulation and a reduction in intra-hepatic glycogen levels, primarily attributed to the decline in PPARα expression. Conversely, in DIO mice, the inhibition of Mof led to an improvement in hepatic TG accumulation and blood glucose levels, which can be attributed to the inhibition of mTOR phosphorylation. These findings provide evidence supporting Mof as a potential therapeutic target for addressing disturbances in lipid metabolism associated with NAFLD.

RESULTS

Mof and H4K16ac expressions were down-regulated in DIO livers

Significant hepatic lipid accumulation, impaired glycogen storage, and fatty degeneration were observed in the livers of DIO mice (Figures 1A–1C). The quantification of the Oil-O staining results was performed by calculating the ratio of positive stain areas to the total valid areas (Figure S4A). Furthermore, impaired glucose tolerance and insulin tolerance were reflected in DIO mice through the use of IPGTT (Figure 1D) and IPITT (Figure 1E) reflected impaired glucose tolerance and insulin tolerance, while biochemical analysis revealed elevated serum TG (Figure 1F) and cholesterol (Figure 1G) levels. Notably, DIO mice exhibited a substantial increase in intrahepatic TG levels, which is a key characteristic of NAFLD (Figure 1H). The elevation of ALT (Figure 1I) and AST (Figure 1J) indicated hepatocyte damage. Additionally, disturbances in lipid, glucose, and amino acid metabolism, as well as autophagy, were observed in NAFLD.[1,6] Western blot analysis revealed a decrease in the expression levels of Cps1, Gck, and PPARα in the livers of DIO subjects, indicating a reduction in the activity of these enzymes involved in the urea cycle, glucose, and lipid metabolism (Figures 1K and 1L). Dysregulation of autophagy was evident through alterations in the markers LC3, p62, and Atg7 (Figure 1M).

Down-regulation of Mof expression was observed in DIO livers through western blotting (Figure 1K) and immunohistochemistry (IHC) staining (Figure 1N), while IF staining demonstrated a decrease in H4K16ac deposition (Figure 1O). q-PCR analysis confirmed the down-regulation of *Mof* mRNA (Figure S1A). To investigate the down-regulation of *Mof* expression in DIO mice, we conducted ChIP-qPCR analysis to detect the presence of H3K27ac, H3K4me3, and H3K27me3 on the Mof promoter. In DIO mice, we observed a decrease in H3K4me3 enrichment, which is indicative of reduced Mof transcription. Conversely, H3K27ac enrichment, another marker of transcriptional activation, was up-regulated, while H3K27me3 enrichment, a marker of transcriptional silencing, was down-regulated (Figure S1B). These findings suggest that the down-regulation of H3K4me3 enrichment may play a crucial role in regulating Mof transcription under high-fat diet conditions.

Hepatic Mof expression was closely related to NAFLD and lipid metabolism

In order to gain insight into the alteration of Mof expression in human liver disease, an analysis was conducted on the data obtained from GSE126848.[29] The findings revealed a consistent decrease in KAT8 mRNA levels from normal body weight to NASH, suggesting a close association between hepatic Mof expression and the progression of NAFLD (Figure S1C).

The re-analysis of transcriptional data from Mof-deficient mice liver tissues demonstrated the regulatory influence of Mof on key genes involved in amino acid, lipid, and glucose metabolism (Figure S1D). Kyoto Encyclopedia of Genes and Genomes (KEGG) annotation highlighted the involvement of Mof in autophagy, fatty acid metabolism, glycolysis/gluconeogenesis, and notably, the PPAR signaling pathway, and PI3K-AKT signaling pathway (Figure S1E). Among genes related to lipid, carbohydrate, and amino acid metabolism, Mof exhibited a significant influence on lipid metabolism, resulting in alterations in 217 (8.15%) genes (Figure S1F). Subsequently, a comparison of differentially expressed genes between GSE126848and GSE106369revealed a substantial overlap, indicating a strong association between hepatic Mof expression, NAFLD, and lipid metabolism (Figure S1G).

Mof knockdown contributed to hepatic metabolic alterations

To gain a comprehensive understanding of Mof's impact on the liver *in vivo*, we generated 4-OHT induced Mof deficient Mof $^{flox/flox}$; ERT Cre mice (Figure 2A). The deficiency of hepatic Mof expression was confirmed, and both H4K16ac and PPARα expressions were down-regulated (Figure 2B). Due to the liver's pivotal role in lipid and carbon carbohydrate metabolism, we conducted a biochemical analysis to examine the levels of serum and intra-hepatic TG and cholesterol. Additionally, we employed Oil-O and Periodic acid Schiff (PAS) staining techniques to assess hepatic lipid and glycogen storage, respectively. The results of the biochemical tests revealed a decrease in serum TG (Figure 2C) but a significant increase in intra-hepatic TG in Mof-deficient mice (Figure 2D), indicating a disruption in hepatic TG metabolism. Furthermore, there was an observed tendency of increased serum cholesterol levels ($p = 0.0760$) (Figure 2E), accompanied by enhanced intrahepatic cholesterol levels (Figure 2F). In terms of amino acids, we specifically measured the level of alanine, which was reported to be essential for glucagon resistance and glucose metabolism. There were no significant alterations observed in the levels of serum and intra-hepatic alanine (Figures 2G and 2H). A previous study suggested that deficiency of Mof could potentially affect liver damage, prompting us to assess the levels of ALT and AST. Knockdown of Mof led to elevated ALT levels (Figure 2I) while AST levels remained unaffected. In addition to biochemical measurements, PAS and Oil-O staining also demonstrated increased lipid accumulation and decrease glycogen storage in Mof-deficient mice (Figures 2J and 2K). Quantification of Oil-O staining indicated elevated hepatic lipid accumulation in Mof-deficient mice (Figure S4B).

Mof played distinct roles in lipid metabolism via PPARα or mTOR signaling pathways under different circumstances

In order to further elucidate the impact of Mof and H4K16ac on lipid metabolism, we employed the Mof acetyltransferase inhibitor, mg149. When mg149 was administrated to AML 12 cells, Oil-O staining revealed an increase in lipid accumulation (Figures 3A and S4C). Intriguingly, when PA was added, mg149 played a constructive role in diminishing intracellular lipid deposits (Figures 3B and S4D), indicating Mof played distinct roles in lipid metabolism under different circumstances. KEGG annotation analysis showed that Mof deficiency affects the PPAR signaling pathway, and further analysis of raw data from GSE106369revealed down-regulation of only PPARα in Mof deficient liver, with no significant changes in PPARγ or PPARδ. Additionally, our previous research demonstrated that Mof influences mTOR phosphorylation.[26,27] Therefore, our focus was directed toward investigating the role of PPARα and mTOR. When mg149 was added to the AML 12 cells, there was a decrease in the expression of H4K16ac, but not H4K8ac, indicating the specific inhibition of Mof by mg149 (Figure 3C). The administration of mg149 did not have a noticeable effect on other histone acetylation markers, such as H3K27ac, H3K9ac, H2BK5ac, H2BK20ac, H3K23ac, and H3K18ac (Figure S2A). The reduction in H4K16ac levels was comparable between mg149 administration and Mof knockdown mediated by si-RNA (Figures 3C and S2B). As a positive control for H4K16ac-mediated gene expression, LC3, a well-established gene, was examined.[16,26,30] PPARα and *p*-mTOR/mTOR levels were decreased, while LC3 II/I ratio increased in mg149-treated cells compared to control cells (Figure 3C). The expressions of PPARα, LC3, and H4K16ac were observed to be down-regulated in Mof knockdown cells (Figure S2B). Decreased PPARα expression is known to play a crucial role in lipid metabolism, particularly in reducing fatty acid oxidation levels. Therefore, in its natural state, Mof inhibition promotes lipid accumulation by reducing PPARα expression.

When PA was administrated to AML 12 cells, the expression levels of Mof, H4K16ac, and PPARα were all down-regulated and mTOR was activated, resembling the conditions observed in high-fat diet-induced obese mice (Figure 3D). Subsequently, upon further administration of mg149, the level of *p*-mTOR/mTOR significantly decreased (Figure 3E). The inhibition of the mTOR signaling pathway has been extensively studied for its beneficial effects on lipid metabolism. In hepatic cells treated with PA, Mof has been found to play a distinct role in reducing intra-cellular lipid deposits by decreasing *p*-mTOR/mTOR levels.

The mechanism of Mof regulated PPARα and mTOR phosphorylation

We conducted Oil-O staining on AML 12 cells treated with mg149 alone or in combination with the PPARα agonist, wy-14643. Interestingly, wy-14643 was able to effectively reverse the lipid accumulation induced by mg149 (Figure 4A; Figure S4E). Therefore, our focus shifted toward understanding how Mof regulates PPARα. Mof primarily regulates metabolic and other important biological processes through two main mechanisms. One approach involves the regulation of gene expression through the Mof-H4K16ac pathway, while the other involves the acetylation of non-histones by Mof, which in turn regulates the activity of its target. Previous research has shown that Sirt1 deacetylates PPARα, leading us to hypothesize that Mof may also influence the acetylation of PPARα.[31] Through Co-IP analysis, we confirmed the binding between

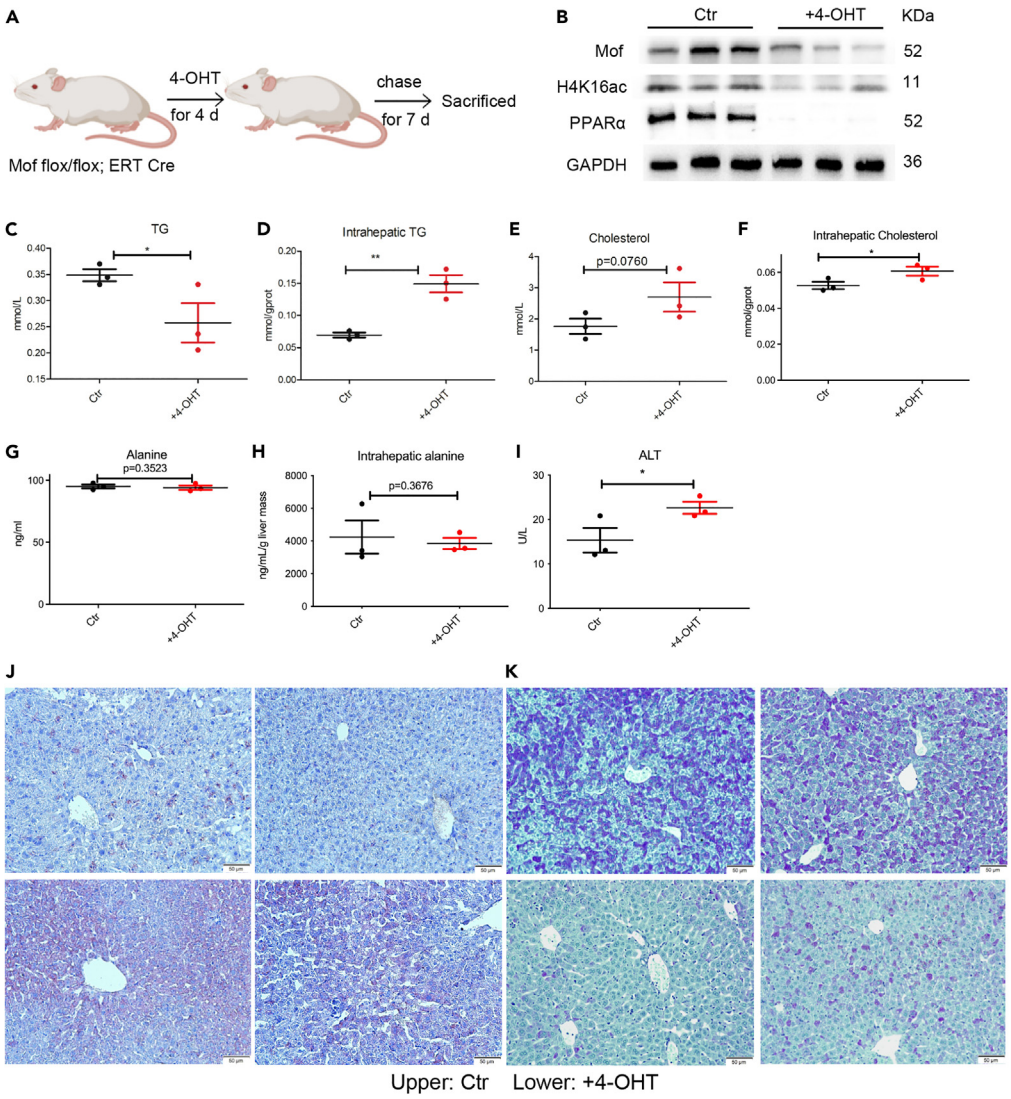

Figure 2. Mof knockdown contributed to hepatic metabolic alterations

(A) The flow-chart illustrating the deficiency of Mof induced by 4-OHT.

(B) The results obtained from western blotting demonstrated the knockdown of Mof and decreased levels of PPARα and H4K16ac (n = 3).

(C and D) The levels of serum and intrahepatic TG were measured (n = 3).

(E and F) The levels of cholesterol were measured (n = 3).

(G and H) The levels of alanine were measured (n = 3).

(I) The level of ALT was measured (n = 3).

(J and K) PAS staining and Oil-O staining revealed increased lipid accumulation and decreased glycogen storage in the livers deficient in Mof. Scale bar: 50 μm. See also Figure S4B.

Graph data were presented as mean ± SEM. n represents the number of mouse. *p < 0.05, **p < 0.01 (Student's *t* test).

Mof and PPARα (Figure 4B), and vice versa (Figure 4C). Subsequently, we observed the acetylation of PPARα, as evidenced by the presence of ac-lysine (Ac-K) in conjunction with PPARα (Figure 4D). Upon the addition of mg149 to AML 12, the co-immunoprecipitation (coIP) analysis revealed a reduction in Ac-K associated with PPARα, (Figure 4E) suggesting that Mof plays a role in regulating the acetylation level of PPARα. We conducted a mass spectrum assay to investigate the acetylation of lysine residues in PPARα (PXD046231). Through this assay, we identified five acetylated lysines in PPARα (K196, K252, K266, K257, and K232) (Figure S2C). In order to determine if these lysines are acetylated by Mof, we utilized the GPS-PAIL 2.0 tool to predict PPARα acetylation sites and acetyltransferase activity.[32,33] It was found that K196 was not a conserved acetylation site. Although the prediction score for K252 was low, it was conserved in both mice and humans. K266 was also conserved, but the prediction score was 0, suggesting that it may not be a target for Mof-mediated acetylation. K257 and K232 were found to be conserved and the predication scores indicated that they were the targets of Mof (Figure S2D). Therefore, it can be inferred that PPAR

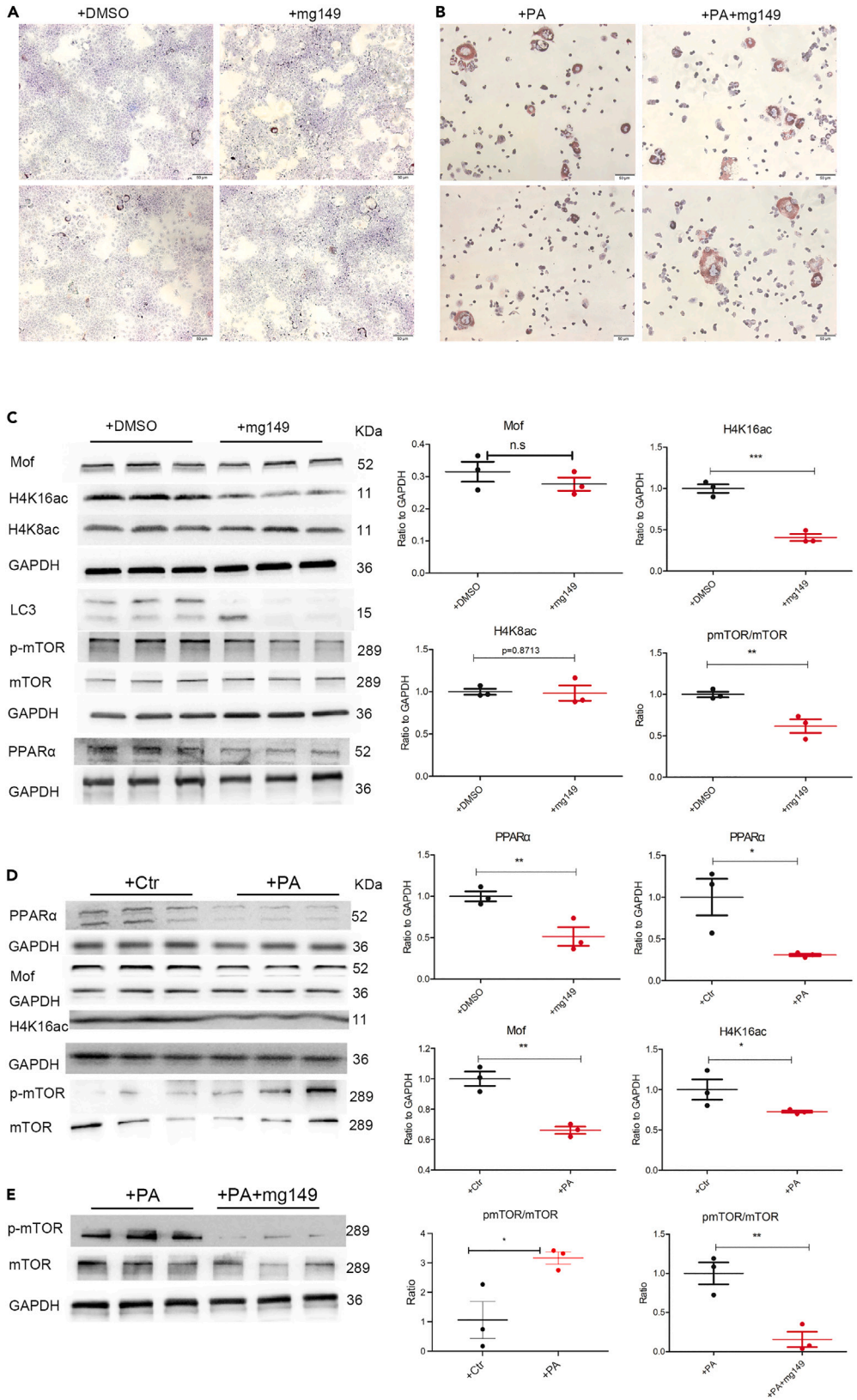
A
+DMSO
+mg149
B
+PA
+PA+mg149
C
+DMSO
+mg149
KDa
Mof
52
H4K16ac
11
H4K8ac
11
GAPDH
36
LC3
15
p-mTOR
289
mTOR
289
GAPDH
36
PPARα
52
GAPDH
36
Mof
n.s
Ratio to GAPDH
H4K16ac
***
H4K8ac
p=0.8713
pmTOR/mTOR
**
Ratio
D
+Ctr
+PA
KDa
PPARα
52
GAPDH
36
Mof
52
GAPDH
36
H4K16ac
11
GAPDH
36
p-mTOR
289
mTOR
289
PPARα
**
*
Mof
**
H4K16ac
*
E
+PA
+PA+mg149
p-mTOR
289
mTOR
289
GAPDH
36
pmTOR/mTOR
*
**

Figure 3. Mof played distinct roles in lipid metabolism via PPARα or mTOR signaling pathway under different circumstances

(A) AML 12 cells were subjected to Oil-O staining following treatment with either DMSO or mg149. Scale bar: 50 μm. See also Figure S4C.

(B) Oil-O staining was performed on AML 12 cells treated with PA + DMSO or PA + mg149. Scale bar: 50 μm. See also Figure S4D.

(C) The effect of mg149 on H4K16ac, PPARα, LC3, and mTOR was assessed using western blotting (n = 3). GAPDH was the loading control, with quantification in the right panel.

(D) Western blotting analysis revealed the influence of PA on Mof, H4K16ac, *p*-mTOR, mTOR, and PPARα (n = 3). GAPDH was the loading control, with quantification in the right panel.

(E) Western blotting demonstrated the impact of mg149 on mTOR in AML 12 cells treated with PA (n = 3). GAPDH was the loading control, with quantification in the right panel.

Graph data were presented as mean ± SEM. n represents the number of western blotting data. *p < 0.05, **p < 0.01, ***p < 0.001 (Student's *t* test).

alpha K257 and K232 were the acetylated lysine targets of Mof (Figure S2E). Our data provided evidence that PPARα was a non-histone target of Mof. In order to assess the impact of Mof acetyltransferase inhibitor on PPARα transcriptional activity, we measured the mRNA levels of well-established downstream genes, such as *acot1*, *cpt1a*, *fabp1*, and *hmgcs1*, and observed a down-regulation of these genes in

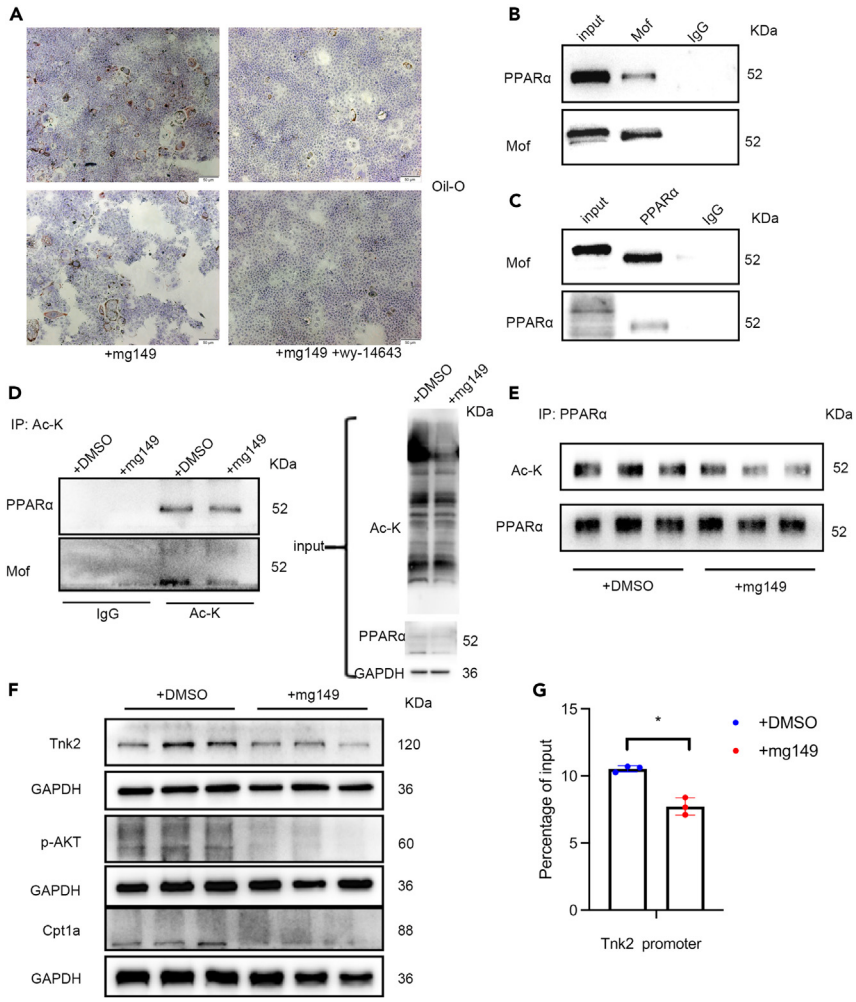

Figure 4. The mechanism of Mof regulated PPARα and mTOR phosphorylation

(A) AML 12 cells were subjected to Oil-O staining following treatment with mg149 or mg149+wy-14643. Scale bar: 50 μm. See also Figure S4E.

(B and C) Co-immunoprecipitation was performed to investigate the interaction between PPARα and Mof (n = 1).

(D) Acetylated lysine residues were identified in PPARα (n = 1).

(E) Administration of mg149 resulted in a reduction of acetylated lysine residues in PPARα (n = 3).

(F) Treatment with mg149 led to a decrease in the expression of Tnk2, Cpt1a, and *p*-AKT (n = 3).

(G) Chromatin immunoprecipitation followed by q-PCR revealed a down-regulation of H4K16ac deposition on the Tnk2 promoter in mg149-treated AML 12 cells (n = 3).

Graph data were presented as mean ± SEM. Each point represents an individual ChIP-qPCR data. *p < 0.05 (Student's *t* test).

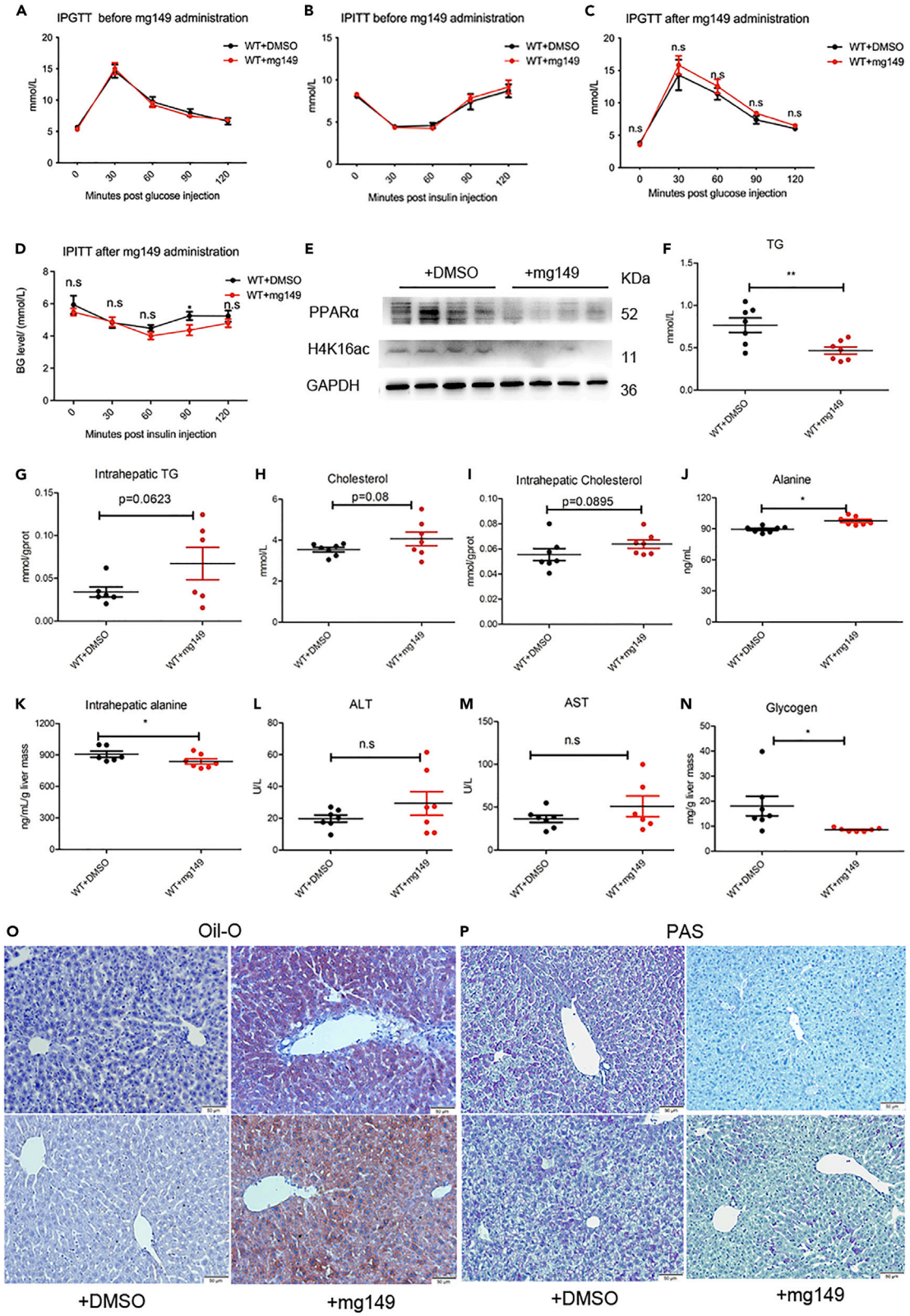
A
IPGTT before mg149 administration
mmol/L
Minutes post glucose injection
WT+DMSO
WT+mg149
B
IPITT before mg149 administration
mmol/L
Minutes post insulin injection
C
IPGTT after mg149 administration
n.s
D
IPITT after mg149 administration
BG level/ (mmol/L)
E
+DMSO
+mg149
KDa
PPARα
H4K16ac
GAPDH
52
11
36
F
TG
**
G
Intrahepatic TG
p=0.0623
mmol/gprot
H
Cholesterol
p=0.08
I
Intrahepatic Cholesterol
p=0.0895
J
Alanine
*
ng/mL
K
Intrahepatic alanine
ng/mL/g liver mass
L
ALT
U/L
M
AST
N
Glycogen
mg/g liver mass
O
Oil-O
P
PAS
+DMSO
+mg149

Figure 5. Impact of Mof inhibition on wild-type hepatic metabolism

(A and B) IPGTT and IPITT of untreated WT mice (n = 7).
(C and D) IPGTT and IPITT of DMSO or mg149 administrated WT mice (n = 7).
(E) Western blotting showed that mg149 treatment led to decreased hepatic PPARα and H4K16ac expressions (n = 4).
(F) Measurements of serum TG levels of WT + DMSO and WT + mg149 groups (n = 7).
(G) Measurements of intra-hepatic TG levels of WT + DMSO and WT + mg149 groups (n = 6).
(H) Measurements of serum cholesterol levels of WT + DMSO and WT + mg149 groups (n = 7).
(I) Measurements of intra-hepatic cholesterol levels of WT + DMSO and WT + mg149 groups (n = 7).
(J) Measurements of serum alanine levels of WT + DMSO and WT + mg149 groups (n = 7).
(K) Measurements of intra-hepatic alanine levels of WT + DMSO and WT + mg149 groups (n = 6–7).
(L–M) ALT and AST between WT + DMSO and WT + mg149 groups showed no difference (n = 6–7).
(N) Biochemical analysis showed that in mg149-treated WT mice, liver glycogen level was decreased (n = 7).
(O) Oil-O staining indicated more lipid deposits in mg149-administrated WT mice. Scale bar: 50 μm. See also Figure S4F.
(P) PAS staining indicated less glycogen in mg149-administrated WT mice.
Graph data were presented as mean ± SEM. n represents the number of mouse. *p < 0.05, **p < 0.01 (Student's *t* test).

mg149-treated AML 12 cells (Figure S2F). Consequently, the protein level of Cpt1a in AML 12 cells treated with mg149 exhibited a decrease (Figure 4F). These findings suggest that mg149 has the ability to diminish the activity of PPARα as a transcription factor.

In relation to mTOR phosphorylation, although the KEGG annotation of the Mof-deficient liver did not specifically focus on the mTOR signaling pathway, it was observed that the upstream regulator of mTOR, AKT, was significantly impacted (Figure S1E). Previous research conducted by our team has demonstrated that Mof regulates *p*-AKT through Tnk2.[34] Therefore, the expression of Tnk2 in mg149-treated AML 12 cells was assessed, revealing a reduction in both Tnk2 and *p*-AKT expression upon administration of mg149 (Figure 4F). q-PCR analysis also revealed a significant reduction in Tnk2 mRNA expression in AML 12 cells treated with mg149 (Figure S2F). ChIP-qPCR demonstrated the presence of H4K16ac deposits in the promoter region of Tnk2 (Figure S2G). Notably, in mg149-treated AML12 cells, the deposition of H4K16ac on the Tnk2 promoter was observed to be down-regulated (Figure 4G). Given that H4K16ac is widely recognized as a marker for transcriptional activation, the diminished presence of H4K16ac deposits suggests a decrease in Tnk2 promoter activity. When mg149 was further added to PA-treated AML 12 cells, decreased expressions of Tnk2 and *p*-AKT were observed (Figure S2H). Consequently, it can be inferred that Mof plays a regulatory role in mTOR phosphorylation through the Tnk2-Akt-mTOR pathway.

Impact of Mof inhibition on wild-type hepatic metabolism

The findings from *in vitro* experiments and studies conducted on Mof-deficient mice demonstrated that inhibiting or reducing Mof expression under normal conditions resulted in increased accumulation of lipids in the liver. To investigate this further, we injected wild type (WT) mice with mg149 to replicate the observed phenotype. Prior to mg149 administration, both groups of mice exhibited similar results in terms of IPGTT (Figure 5A) and IPITT (Figure 5B). Consistent with our previous findings, the administration of mg149 in WT mice did not affect glucose tolerance (Figure 5C). However, it did lead to a slower restoration of normal glucose levels following insulin injection, which was attributed to a decrease in glucagon receptor expression (Figure 5D).[27] The western blot analysis of liver tissues revealed that treatment with mg149 resulted in a decrease in H4K16ac and PPARα expressions (Figure 5E). This was further supported by biochemical analysis, which demonstrated similar changes to those observed in Mof-deficient mice. Serum TG levels were reduced (Figure 5F), while intrahepatic TG levels showed a tendency to increase ($p = 0.0623$) (Figure 5G). However, there were no statistically significant alterations in both serum and intrahepatic cholesterol levels (Figures 5H and 5I). Intriguingly, Mof inhibition led to an increase in serum alanine levels (Figure 5J) but a decrease in intrahepatic alanine levels (Figure 5K). The levels of ALT and AST did not differ between the control and mg149 group, which may be attributed to the relatively short duration of mg149 administration (Figures 5L–5M). Similar to Mof-deficient mice, the hepatic lipid accumulation was significantly increased (Figures 5N and S4F) and glycogen storage was markedly reduced (Figure 5O), as evidenced by chemical glycogen measurements (Figure 5P).

Impact of Mof inhibition on DIO hepatic metabolism

Our *in vitro* investigation revealed that Mof inhibition exerted distinct effects on normal and PA-treated hepatic cells. Subsequently, we administered mg149 to DIO mice to evaluate the potential therapeutic impact of Mof inhibition on hepatic metabolism. Prior to mg149 administration, no discernible disparity was observed in IPGTT and IPITT (Figures 6A and 6B). However, following mg149 treatment, DIO mice exhibited enhanced glucose tolerance, as indicated by decreased blood glucose levels in 30-, 60-, 90-, and 120-min post glucose challenge (Figure 6C). The administration of mg149 did not have an impact on insulin tolerance, as evidenced by the lack of significant alteration in glucose levels following an insulin challenge between the two groups (Figure 6D). Western blotting analysis revealed a decrease in H4K16ac and LC3, while H4K8ac remained unchanged (Figure 6E). In mg149-treated DIO mice, there was no change in serum TG levels (Figure 6F), but intrahepatic TG levels (Figure 6G) were decreased. Serum cholesterol was decreased (Figure 6H), while intra-hepatic cholesterol was unaltered (Figure 6I). In mg149-treated DIO mice, serum alanine was decreased (Figure 6J), while intra-hepatic alanine was elevated (Figure 6K). The levels of ALT and AST in mg149-treated mice did not show any changes (Figures 6L–6M). The findings of this study demonstrate that the administration of mg149 in DIO mice led to reductions in intrahepatic TG levels, cholesterol levels, and alanine levels. Additionally, it improved glucose tolerance, thereby reversing the hepatic metabolic disturbances observed in obese individuals and those with NAFLD.

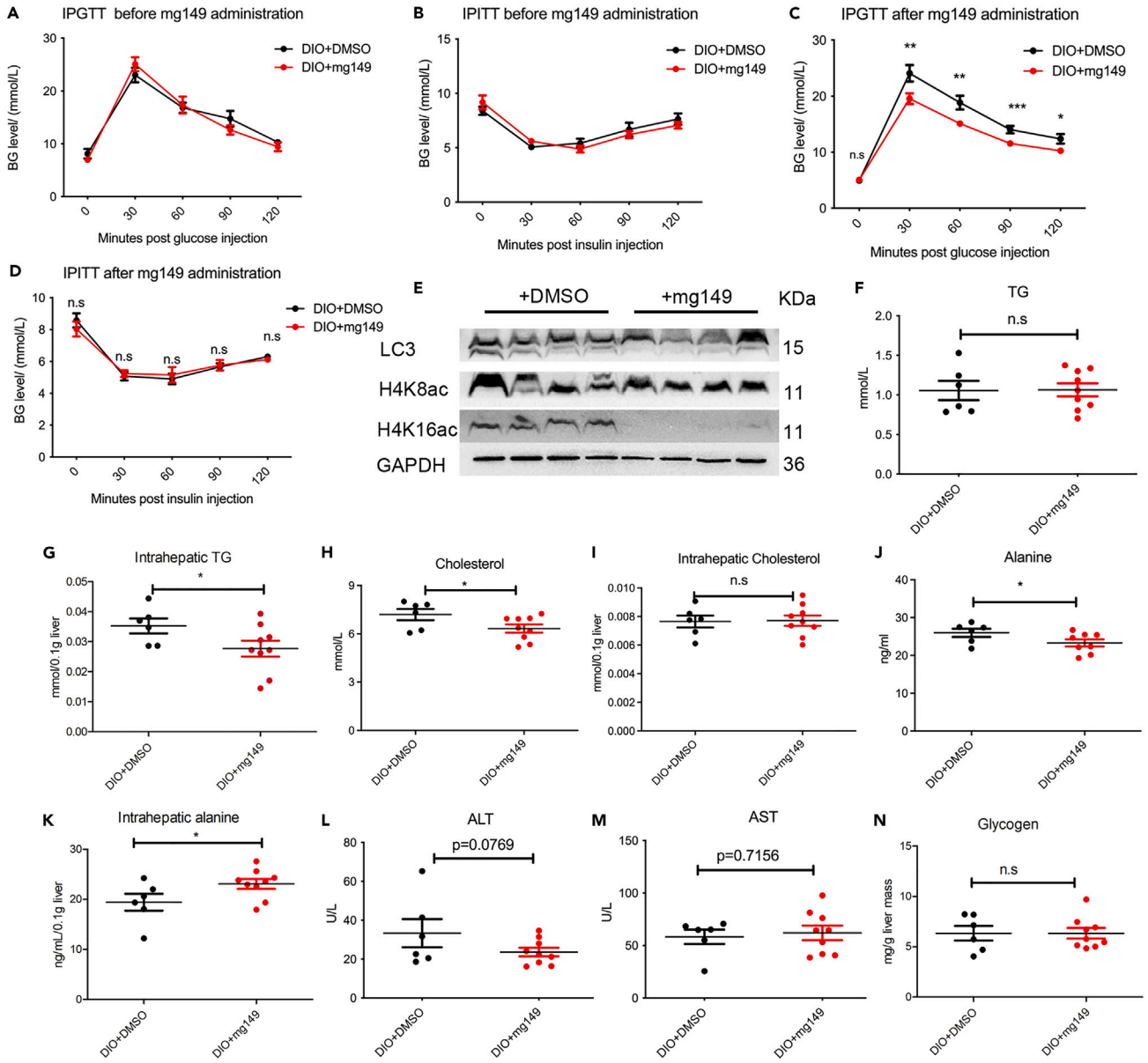

Figure 6. Impact of Mof inhibition on DIO hepatic biochemical analysis

(A and B) IPGTT and IPITT of untreated DIO mice (n = 6 in DIO+DMSO group and n = 10 in DIO+mg149 group).

(C and D) IPGTT and IPITT of DMSO or mg149 administrated DIO mice (n = 6 in DIO+DMSO group and n = 10 in DIO+mg149 group).

(E) Western blotting showed that mg149 treatment led to decreased hepatic LC3 and H4K16ac expressions (n = 4).

(F)Measurements of serum TG levels of DIO+DMSO and DIO+mg149 groups (n = 6 in DIO+DMSO group and n = 9 in DIO+mg149 group).

(G) Measurements of intrahepatic TG levels of DIO+DMSO and DIO+mg149 groups (n = 6 in DIO+DMSO group and n = 9 in DIO+mg149 group).

(H) Measurements of serum cholesterol levels of DIO+DMSO and DIO+mg149 groups (n = 6 in DIO+DMSO group and n = 9 in DIO+mg149 group).

(I) Measurements of intra-hepatic cholesterol levels of DIO+DMSO and DIO+mg149 groups (n = 6 in DIO+DMSO group and n = 9 in DIO+mg149 group).

(J) Measurements of serum alanine levels of DIO+DMSO and DIO+mg149 groups (n = 6 in DIO+DMSO group and n = 8 in DIO+mg149 group).

(K) Measurements of intra-hepatic alanine levels of DIO+DMSO and DIO+mg149 groups (n = 6 in DIO+DMSO group and n = 9 in DIO+mg149 group).

(L and M) ALT (p = 0.0769) and AST (p = 0.7156) between DIO+DMSO and DIO+mg149 groups showed no difference (n = 6 in DIO+DMSO group and n = 9 in DIO+mg149 group).

(N) Glycogen measurement indicated no difference in glycogen storage (n = 6 in DIO+DMSO group and n = 9 in DIO+mg149 group).

Graph data were presented as mean ± SEM. n represents the number of mouse. *p < 0.05, **p < 0.01, ***p < 0.001 (Student's *t* test).

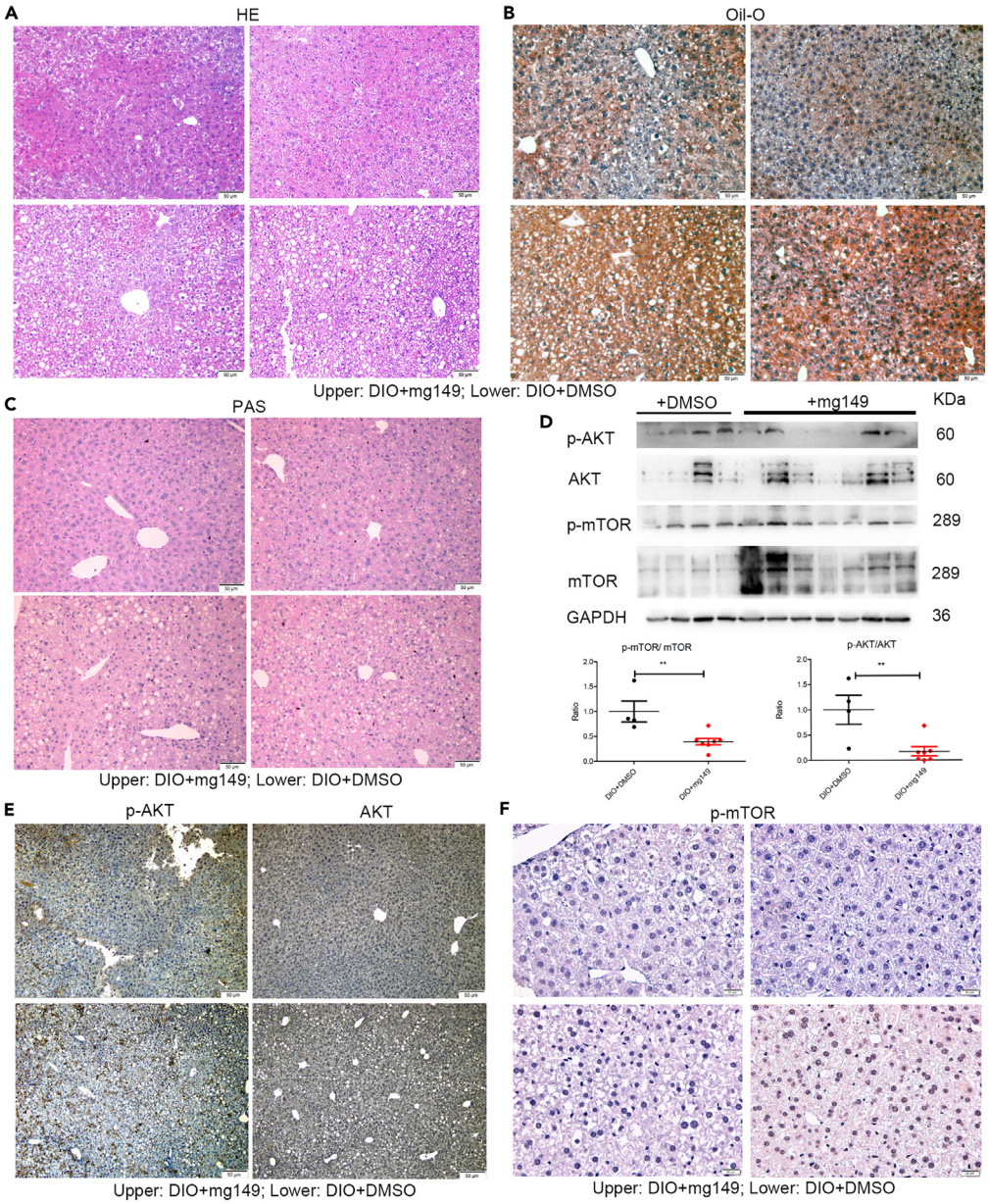

Figure 7. Impact of Mof inhibition on DIO hepatic morphological analysis

(A) HE staining showed smaller lipid droplets in mg149 administrated DIO mice. Scale bar: 50 μm.

(B) Oil-O staining showed less lipid deposit mg149 administrated DIO mice. Scale bar: 50 μm. See also Figure S4G.

(C) PAS staining indicated no difference in glycogen storage. Scale bar: 50 μm.

(D) Western blotting showed decreased *p*-AKT and *p*-mTOR levels (n = 4 in DIO+DMSO group and n = 7 in DIO+mg149 group).

(E) IHC staining showed decreased *p*-AKT levels. Scale bar: 50 μm.

(F) IHC staining showed decreased *p*-mTOR levels. Scale bar: 20 μm.

Graph data were presented as mean ± SEM. n represents the number of mouse. **p < 0.01 (Student's *t* test).

To further elucidate the morphological and metabolic changes, staining techniques were employed. The results of HE staining revealed that the large lipid droplets in mg149-treated DIO livers underwent breakdown into smaller droplets, indicating an enhanced fatty degeneration (Figure 7A). Oil-O staining demonstrated a decrease in intrahepatic lipid content (Figure 7B; Figure S4G), consistent with the findings of an *in vitro* study. Both PAS staining (Figure 7C) and glycogen measurements (Figure 6N) indicated no significant changes in glycogen storage levels. Our previous study demonstrated that Mof inhibition in PA-treated cells had positive effects on lipid metabolism through the mTOR signaling pathway. Western blotting analysis revealed down-regulation of *p*-AKT/AKT and *p*-mTOR/mTOR in mg149-treated DIO mice (Figure 7D), which was further confirmed by IHC staining of *p*-AKT (Figure 7E) and *p*-mTOR (Figure 7F).

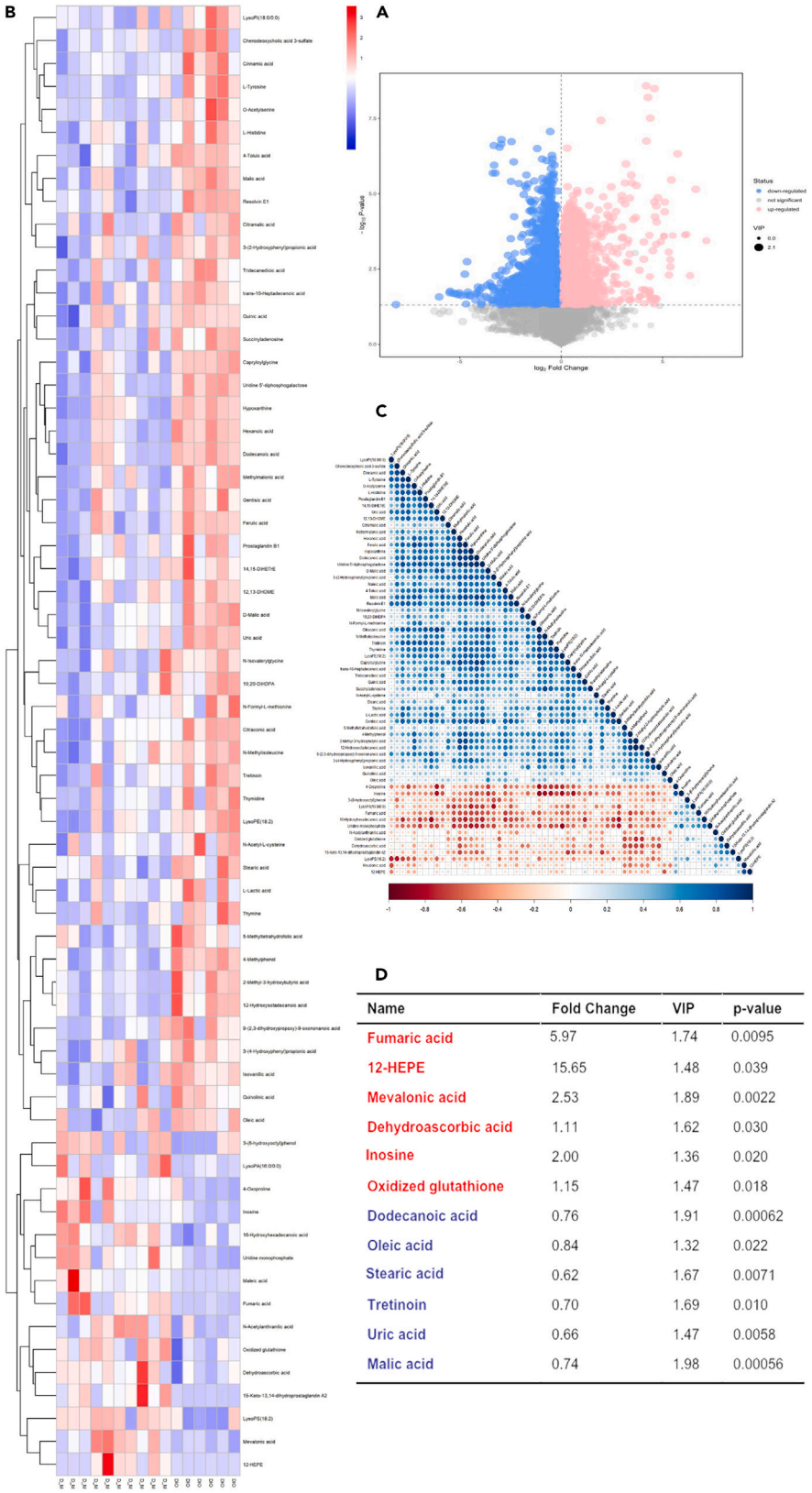

D

Name	Fold Change	VIP	p-value
Fumaric acid	5.97	1.74	0.0095
12-HEPE	15.65	1.48	0.039
Mevalonic acid	2.53	1.89	0.0022
Dehydroascorbic acid	1.11	1.62	0.030
Inosine	2.00	1.36	0.020
Oxidized glutathione	1.15	1.47	0.018
Dodecanoic acid	0.76	1.91	0.00062
Oleic acid	0.84	1.32	0.022
Stearic acid	0.62	1.67	0.0071
Tretinoin	0.70	1.69	0.010
Uric acid	0.66	1.47	0.0058
Malic acid	0.74	1.98	0.00056

Figure 8. Impact of Mof inhibition on the metabonomics of DIO livers

(A and B) Volcano plot and heatmap of metabolites with the altered amount between DIO+DMSO mice liver and DIO+mg149 mice liver (n = 6 in DIO+DMSO group and n = 10 in DIO+mg149 group).

(C) Correlations of altered metabolites.

(D) The table listed the most significant metabolites related with observed phenotype. The variable importance in the projection (VIP) value of each variable in the OPLS-DA model was calculated to indicate its contribution to the classification. Significance was determined using an unpaired Student's *t* test. VIP value > 1 and $p < 0.05$ was considered statistically significant. n represents the number of mouse.

Impact of Mof inhibition on the metabonomics of DIO livers

Both *in vivo* and *in vitro* studies suggested Mof inhibition played distinct roles in the livers of WT and DIO mice. Therefore, we were interested in identifying the specific metabolites that were altered in mg149-treated DIO livers. Hence, a metabonomics analysis was conducted (Metabolomics data have been deposited to the EMBL-EBI MetaboLights database with the identifier MTBLS8423), revealing distinct metabolite features among different groups as depicted in the score scatterplot for principal component analysis (PCA) (Figure S3A).[35] Furthermore, the application of PLS-DA (Figure S3B) and orthogonal partial least-squares discriminant analysis (OPLS-DA) (Figure S3C) analysis demonstrated notable differences in characteristics between mg149-treated and DMSO-treated mice. The volcano plot indicated significant alterations in the quantities of numerous metabolites (Figure 8A), thereby highlighting the variations among them. Additionally, the heatmap (Figure 8B) presented the most significantly changed metabolites, while Figure 8C illustrated the correlations among these metabolites. We listed those involved in the phenotype of mg149-treated DIO mice (Figure 8D). Intriguingly, there was an increase in the concentrations of fumaric acid, 12-HEPE, and inosine, which were strongly associated with an improved metabolic phenotype. Inosine, known for its hepatoprotective properties, accounted for the observed decrease in ALT levels. Fumaric acid (Figure S3D), a widely recognized therapeutic metabolite for psoriasis, plays a crucial role in various metabolic pathways such as the citrate cycle and oxidative phosphorylation.[36,37] Clinical trials have demonstrated the cholesterol-lowering effects of fumaric acid,[38] while animal models have shown its derivatives to effectively mitigate liver injury.[39,40] 12-HEPE acts as a PPAR ligand, and regulates glucose metabolism.[41,42] However, the investigation of these metabolites in the context of NAFLD and lipid metabolism disturbance has been limited. Nonetheless, in DIO mice treated with mg149, the PPAR signaling pathway was affected, including the key metabolite, 9-cis-retinoic acid (Figure S3E). Consistent with the findings from Oil-O staining, the levels of dodecanoic acid, oleic acid, and stearic acid were all significantly reduced (Figure S3F).

DISCUSSION

The relationship between metabolism and acetylation, particularly histone acetylation, suggests that targeting acetylation may hold promise for treating metabolic disorders such as T2DM and NAFLD.[43] Histone acetylation plays a role in regulating gene expression and can have tissue-specific effects.[44] While various therapeutic targets for hepatic lipid metabolism disorder have been proposed, including the mTOR signaling pathway,[9] PPARα,[8] ATP-citrate lyase,[45] and Sirt1,[46] there has been limited research on therapeutic methods targeting histone acetyltransferase.

Our previous research has provided evidence that Mof modulates glucose levels by influencing the mass and hormone secretion of various α-cell subsets.[26] Additionally, inhibiting Mof has shown potential in improving glucose tolerance in DIO mice. In this current study, we have discovered a strong association between Mof and hepatic lipid metabolism. Mof exhibits distinct functions in lipid metabolism depending on the specific circumstances. Notably, the administration of mg149 in DIO mice resulted in reduced intrahepatic TG levels, decreased cholesterol and alanine levels, and enhanced glucose tolerance, effectively reversing the metabolic disturbances in the liver. The data presented in this study indicate that inhibiting Mof holds promise as a potential target for preventing the progression from obesity to NAFLD and diabetes.

Furthermore, our findings suggest that Mof may also serve as a therapeutic target for addressing the disruption of the "liver-α cell axis". In individuals with obesity and NAFLD, there was an observed increase in serum alanine levels.[47] This elevation in serum alanine strongly stimulates α cell proliferation and glucagon secretion, ultimately leading to increased glucogenesis.[5,48] Our previous research demonstrated that inhibiting Mof resulted in a reduction in α cell mass and glucagon levels.[27] In this study, we additionally illustrated that inhibition of Mof in DIO mice resulted in decreased serum alanine levels. Consequently, Mof inhibition effectively counteracts the disruptions of the "liver-α cell axis" from both hepatic and α cell perspectives, thereby highlighting its potential therapeutic significance in metabolic disorders.

However, it is worth noting that the therapeutic benefits of Mof inhibition were less pronounced in WT mice. We substantiated that, in its natural state, Mof governs the acetylation and expression of PPARα, while concurrently observing a down-regulation in the level of *p*-mTOR/mTOR. The findings of our study suggest that in a natural state, PPARα has a dominant influence on lipid metabolism compared to the mTOR signaling pathway. However, when exposed to high-fat stimulation, the mTOR signaling pathway becomes more influential than PPARα. This can be attributed to the fact that mTOR acts as a sensor for nutrient availability and response accordingly. Consequently, inhibiting the mTOR signaling pathway is expected to have more pronounced effects on DIO mice compared to WT mice.[49,50]

Mof-mediated lipid metabolism was also essential for cancer cell behavior. Specifically, in colorectal cancer cells, the acetylation-controlled lipolysis regulated by Mof significantly impacts their invasive and migratory potential. Same to our data, the knockdown of Mof effectively decreased lipid accumulation in conditions treated with PA.[51] Mof-mediated lipid metabolism has been reported to have diverse functions in adipocyte differentiation,[52] stem cell renewal,[24] and pericyte activation,[25] in addition to hepatocytes and colorectal cancer cells. Consistent with our findings, Mof knockdown in its natural state promoted lipid accumulation.[25] Hence, the regulatory role of Mof in lipid metabolism appears to be widespread and crucial in various domains beyond metabolic disorders.

One of the limitations of our study is the unavailability of mice with long-term administration of mg149. The administration of mg149 for a duration of two weeks resulted in statistically significant, albeit not dramatic, alterations in metabolites and insulin sensitivity. Our previous research demonstrated that Mof-deficient mice displayed aggravated insulin resistance. However, both our previous work and the current study indicate that insulin resistance in mg149-treated mice remained unaltered. The reduction in intra-hepatic TG levels should theoretically enhance insulin sensitivity. Nevertheless, we also observed a decrease in *p*-AKT/AKT levels in mg149-treated DIO mice. Theoretically, a decrease in *p*-Akt levels will result in an increase in nuclear retention of Foxo1, thereby promoting gluconeogenesis, as observed in cases of insulin resistance.[53] Further investigation is warranted to explore the potential significant effects of long-term administration of mg149 on metabolic changes and insulin sensitivity.

Limitations of the study

Our data did not elucidate the underlying mechanism through which Mof exerts its role in specific metabolic pathways. Additionally, we employed 4-OHT induced global Mof deficient mice instead of liver-specific Mof knockout mice to demonstrate the impact of Mof on metabolism *in vivo*. Furthermore, the duration of inhibiting Mof acetyltransferase activity using mg149 *in vivo* was limited to 2–3 weeks. A longer duration may provide a more robust effect and potentially reveal any side effects. The effect of mg149 on H4K16ac exhibits consistency across various studies, as evidenced by the reduction in H4K16ac levels upon mg149 administration. Our study, along with certain others, demonstrates no alteration in Mof expression following mg149 administration, which might be due to that mg149 inhibited Mof activity but not expression. However, longer duration or higher concentration of mg149 administration might have an impact on Mof expression, which deserves further study. In this manuscript, our findings indicate that short-term treatment with mg149 did not significantly affect the insulin sensitivity of DIO mice, despite observing a reduction in hepatic lipid accumulation and improved glucose tolerance. This particular phenotype may be attributed to the additional effects of mg149 outside of the liver. Our previous study demonstrated that administering mg149 to DIO mice resulted in elevated insulin levels following a glucose challenge. Therefore, the systematic studies on the role of Mof in metabolism-related organs warrant further investigation. An additional constraint of this study pertained to the exclusive utilization of palmitic acid as the inducer for lipid accumulation, with the omission of other potential inducers, such as oleic acid. Furthermore, it is imperative to investigate additional metabolic pathways, beyond the PPARα and mTOR pathways, that may potentially contribute to the metabolic phenotype mediated by Mof, warranting further research. According to the findings of this study, the impact of Mof knockdown on hepatic glycogen storage in wild-type mice was found to be highly significant, necessitating further investigation. Furthermore, our manuscript also reported changes in amino acid levels, although a comprehensive examination of the urea cycle process was not conducted. Mof has been previously identified as a crucial factor in mitochondrial function, which is integral to hepatic metabolism. However, this manuscript lacks a thorough analysis of the mitochondrial dysfunction induced by Mof deficiency or mg149 administration, which should be addressed in our forthcoming research.

STAR★METHODS

Detailed methods are provided in the online version of this paper and include the following:

SUPPLEMENTAL INFORMATION

Supplemental information can be found online at https://doi.org/10.1016/j.isci.2023.108446.

ACKNOWLEDGMENTS

This work was supported by the National Natural Science Foundation of China [grant number 82200915, 81900756, 82270845], the Natural Science Foundation of Shandong Province [grant number ZR2022QH232, ZR2022MH003].

AUTHOR CONTRIBUTIONS

Conceptualization: X.G. and L.C.; methodology: X.L., X.Z., and J.L.; investigation: X.G., L.X., C.W., and J.L.; resources: X.L.; data curation: X.G. and K.L.; writing-original draft: X.G., K.L., and J.L.; writing-review & editing: X.G. and K.L.; supervision: L.C. and X.H. funding acquisition: X.G., K.L., and X.L.

DECLARATION OF INTERESTS

The authors declare no competing interests.

INCLUSION AND DIVERSITY

We support inclusive, diverse, and equitable conduct of research.

Received: April 17, 2023
Revised: September 11, 2023
Accepted: November 9, 2023
Published: November 14, 2023

REFERENCES

1. Jones, J.G. (2016). Hepatic glucose and lipid metabolism. Diabetologia *59*, 1098–1103.
2. Gluchowski, N.L., Becuwe, M., Walther, T.C., and Farese, R.V., Jr. (2017). Lipid droplets and liver disease: from basic biology to clinical implications. Nat. Rev. Gastroenterol. Hepatol. *14*, 343–355.
3. Tilg, H., Moschen, A.R., and Roden, M. (2017). NAFLD and diabetes mellitus. Nat. Rev. Gastroenterol. Hepatol. *14*, 32–42.
4. Gar, C., Haschka, S.J., Kern-Matschilles, S., Rauch, B., Sacco, V., Prehn, C., Adamski, J., Seissler, J., Wewer Albrechtsen, N.J., Holst, J.J., and Lechner, A. (2021). The liver-alpha cell axis associates with liver fat and insulin resistance: a validation study in women with non-steatotic liver fat levels. Diabetologia *64*, 512–520.
5. Dean, E.D., Li, M., Prasad, N., Wisniewski, S.N., Von Deylen, A., Spaeth, J., Maddison, L., Botros, A., Sedgeman, L.R., Bozadjieva, N., et al. (2017). Interrupted Glucagon Signaling Reveals Hepatic α Cell Axis and Role for L-Glutamine in α Cell Proliferation. Cell Metab. *25*, 1362–1373.e5.
6. Wewer Albrechtsen, N.J., Pedersen, J., Galsgaard, K.D., Winther-Sørensen, M., Suppli, M.P., Janah, L., Gromada, J., Vilstrup, H., Knop, F.K., and Holst, J.J. (2019). The Liver-α-Cell Axis and Type 2 Diabetes. Endocr. Rev. *40*, 1353–1366.
7. Montagner, A., Polizzi, A., Fouché, E., Ducheix, S., Lippi, Y., Lasserre, F., Barquissau, V., Régnier, M., Lukowicz, C., Benhamed, F., et al. (2016). Liver PPARα is crucial for whole-body fatty acid homeostasis and is protective against NAFLD. Gut *65*, 1202–1214.
8. Smati, S., Polizzi, A., Fougerat, A., Ellero-Simatos, S., Blum, Y., Lippi, Y., Régnier, M., Laroyenne, A., Huillet, M., Arif, M., et al. (2022). Integrative study of diet-induced mouse models of NAFLD identifies PPARα as a sexually dimorphic drug target. Gut *71*, 807–821.
9. Gosis, B.S., Wada, S., Thorsheim, C., Li, K., Jung, S., Rhoades, J.H., Yang, Y., Brandimarto, J., Li, L., Uehara, K., et al. (2022). Inhibition of nonalcoholic fatty liver disease in mice by selective inhibition of mTORC1. Science *376*, eabf8271.
10. Pawlak, M., Lefebvre, P., and Staels, B. (2015). Molecular mechanism of PPARα action and its impact on lipid metabolism, inflammation and fibrosis in non-alcoholic fatty liver disease. J. Hepatol. *62*, 720–733.
11. Xu, J., Xiao, G., Trujillo, C., Chang, V., Blanco, L., Joseph, S.B., Bassilian, S., Saad, M.F., Tontonoz, P., Lee, W.N.P., and Kurland, I.J. (2002). Peroxisome proliferator-activated receptor alpha (PPARalpha) influences substrate utilization for hepatic glucose production. J. Biol. Chem. *277*, 50237–50244.
12. Han, J., and Wang, Y. (2018). mTORC1 signaling in hepatic lipid metabolism. Protein Cell *9*, 145–151.
13. Li, S., Brown, M.S., and Goldstein, J.L. (2010). Bifurcation of insulin signaling pathway in rat liver: mTORC1 required for stimulation of lipogenesis, but not inhibition of gluconeogenesis. Proc. Natl. Acad. Sci. USA *107*, 3441–3446.
14. Taipale, M., Rea, S., Richter, K., Vilar, A., Lichter, P., Imhof, A., and Akhtar, A. (2005). hMOF histone acetyltransferase is required for histone H4 lysine 16 acetylation in mammalian cells. Mol. Cell Biol. *25*, 6798–6810.
15. Singh, M., Bacolla, A., Chaudhary, S., Hunt, C.R., Pandita, S., Chauhan, R., Gupta, A., Tainer, J.A., and Pandita, T.K. (2020). Histone Acetyltransferase MOF Orchestrates Outcomes at the Crossroad of Oncogenesis, DNA Damage Response, Proliferation, and Stem Cell Development. Mol. Cell Biol. *40*. e002322-20.
16. Füllgrabe, J., Lynch-Day, M.A., Heldring, N., Li, W., Struijk, R.B., Ma, Q., Hermanson, O., Rosenfeld, M.G., Klionsky, D.J., and Joseph, B. (2013). The histone H4 lysine 16 acetyltransferase hMOF regulates the outcome of autophagy. Nature *500*, 468–471.
17. Huai, W., Liu, X., Wang, C., Zhang, Y., Chen, X., Chen, X., Xu, S., Thomas, T., Li, N., and Cao, X. (2019). KAT8 selectively inhibits antiviral immunity by acetylating IRF3. J. Exp. Med. *216*, 772–785.
18. Sykes, S.M., Stanek, T.J., Frank, A., Murphy, M.E., and McMahon, S.B. (2009). Acetylation of the DNA binding domain regulates transcription-independent apoptosis by p53. J. Biol. Chem. *284*, 20197–20205.
19. Chen, Z., Ye, X., Tang, N., Shen, S., Li, Z., Niu, X., Lu, S., and Xu, L. (2014). The histone acetylranseferase hMOF acetylates Nrf2 and regulates anti-drug responses in human non-small cell lung cancer. Br. J. Pharmacol. *171*, 3196–3211.
20. Ke, W., Reed, J.N., Yang, C., Higgason, N., Rayyan, L., Wählby, C., Carpenter, A.E., Civelek, M., and O'Rourke, E.J. (2021). Genes in human obesity loci are causal obesity genes in C. elegans. PLoS Genet. *17*, e1009736.
21. Du, Z., Ma, L., Qu, H., Chen, W., Zhang, B., Lu, X., Zhai, W., Sheng, X., Sun, Y., Li, W., et al. (2019). Whole Genome Analyses of Chinese Population and De Novo Assembly of A Northern Han Genome. Dev. Reprod. Biol. *17*, 229–247.
22. Chatterjee, A., Seyfferth, J., Lucci, J., Gilsbach, R., Preissl, S., Böttinger, L., Mårtensson, C.U., Panhale, A., Stehle, T., Kretz, O., et al. (2016). MOF Acetyl Transferase Regulates Transcription and

Respiration in Mitochondria. Cell *167*, 722–738.e23.
23. Pessoa Rodrigues, C., Chatterjee, A., Wiese, M., Stehle, T., Szymanski, W., Shvedunova, M., and Akhtar, A. (2021). Histone H4 lysine 16 acetylation controls central carbon metabolism and diet-induced obesity in mice. Nat. Commun. *12*, 6212.
24. Khoa, L.T.P., Tsan, Y.C., Mao, F., Kremer, D.M., Sajjakulnukit, P., Zhang, L., Zhou, B., Tong, X., Bhanu, N.V., Choudhary, C., et al. (2020). Histone Acetyltransferase MOF Blocks Acquisition of Quiescence in Ground-State ESCs through Activating Fatty Acid Oxidation. Cell Stem Cell *27*, 441–458.e10.
25. Sheikh, B.N., Guhathakurta, S., Tsang, T.H., Schwabenland, M., Renschler, G., Herquel, B., Bhardwaj, V., Holz, H., Stehle, T., Bondareva, O., et al. (2020). Neural metabolic imbalance induced by MOF dysfunction triggers pericyte activation and breakdown of vasculature. Nat. Cell Biol. *22*, 828–841.
26. Guo, X., Li, D., Song, J., Yang, Q., Wang, M., Yang, Y., Wang, L., Hou, X., Chen, L., and Li, X. (2020). Mof regulates glucose level via altering different α-cell subset mass and intra-islet glucagon-like peptide-1, glucagon secretion. Metabolism *109*, 154290.
27. Guo, X., Cui, C., Song, J., He, Q., Zang, N., Hu, H., Wang, X., Li, D., Wang, C., Hou, X., et al. (2021). Mof acetyltransferase inhibition ameliorates glucose intolerance and islet dysfunction of type 2 diabetes via targeting pancreatic α-cells. Mol. Cell. Endocrinol. *537*, 111425.
28. Lei, H., denDekker, A.D., Li, G., Zhang, Z., Sha, L., Schaller, M.A., Kunkel, S.L., Rui, L., Tao, K., and Dou, Y. (2021). Dysregulation of intercellular signaling by MOF deletion leads to liver injury. J. Biol. Chem. *296*, 100235.
29. Suppli, M.P., Rigbolt, K.T.G., Veidal, S.S., Heebøll, S., Eriksen, P.L., Demant, M., Bagger, J.I., Nielsen, J.C., Oró, D., Thrane, S.W., et al. (2019). Hepatic transcriptome signatures in patients with varying degrees of nonalcoholic fatty liver disease compared with healthy normal-weight individuals. Am. J. Physiol. Gastrointest. Liver Physiol. *316*, G462–G472.
30. Zehender, A., Li, Y.N., Lin, N.Y., Stefanica, A., Nüchel, J., Chen, C.W., Hsu, H.H., Zhu, H., Ding, X., Huang, J., et al. (2021). TGFβ promotes fibrosis by MYST1-dependent epigenetic regulation of autophagy. Nat. Commun. *12*, 4404.
31. Suh, J.H., Kim, K.H., Conner, M.E., Moore, D.D., and Preidis, G.A. (2022). Hepatic PPARα Is Destabilized by SIRT1 Deacetylase in Undernourished Male Mice. Front. Nutr. *9*, 831879.
32. Deng, W., Wang, C., Zhang, Y., Xu, Y., Zhang, S., Liu, Z., and Xue, Y. (2016). GPS-PAIL: prediction of lysine acetyltransferase-specific modification sites from protein sequences. Sci. Rep. *6*, 39787.
33. Li, A., Xue, Y., Jin, C., Wang, M., and Yao, X. (2006). Prediction of Nepsilon-acetylation on internal lysines implemented in Bayesian Discriminant Method. Biochem. Biophys. Res. Commun. *350*, 818–824.
34. Li, D., Yang, Y., Chen, B., Guo, X., Gao, S., Wang, M., Duan, M., and Li, X. (2020). MOF Regulates TNK2 Transcription Expression to Promote Cell Proliferation in Thyroid Cancer. Front. Pharmacol. *11*, 607605.
35. Haug, K., Cochrane, K., Nainala, V.C., Williams, M., Chang, J., Jayaseelan, K.V., and O'Donovan, C. (2020). MetaboLights: a resource evolving in response to the needs of its scientific community. Nucleic Acids Res. *48*, D440–D444.
36. Zhu, Y., Wang, X., Zhu, L., Tu, Y., Chen, W., Gong, L., Pan, T., Lin, H., Lin, J., Sun, H., et al. (2022). Lactobacillus rhamnosus GG combined with inosine ameliorates alcohol-induced liver injury through regulation of intestinal barrier and Treg/Th1 cells. Toxicol. Appl. Pharmacol. *439*, 115923.
37. Módis, K., Gerő, D., Stangl, R., Rosero, O., Szijártó, A., Lotz, G., Mohácsik, P., Szoleczky, P., Coletta, C., and Szabó, C. (2013). Adenosine and inosine exert cytoprotective effects in an in vitro model of liver ischemia-reperfusion injury. Int. J. Mol. Med. *31*, 437–446.
38. Holzer, G., Hoke, M., Sabeti-Sandor, S., Perkmann, T., Rauscher, A., Strassegger, B., Radakovic, S., and Tanew, A. (2021). Disparate effects of adalimumab and fumaric acid esters on cardiovascular risk factors in psoriasis patients: results from a prospective, randomized, observer-blinded head-to-head trial. J. Eur. Acad. Dermatol. Venereol. *35*, 441–449.
39. Abdelrahman, R.S., and Abdel-Rahman, N. (2019). Dimethyl fumarate ameliorates acetaminophen-induced hepatic injury in mice dependent of Nrf-2/HO-1 pathway. Life Sci. *217*, 251–260.
40. Takasu, C., Vaziri, N.D., Li, S., Robles, L., Vo, K., Takasu, M., Pham, C., Farzaneh, S.H., Shimada, M., Stamos, M.J., and Ichii, H. (2017). Treatment with dimethyl fumarate ameliorates liver ischemia/reperfusion injury. World J. Gastroenterol. *23*, 4508–4516.
41. Yamada, H., Oshiro, E., Kikuchi, S., Hakozaki, M., Takahashi, H., and Kimura, K.I. (2014). Hydroxyeicosapentaenoic acids from the Pacific krill show high ligand activities for PPARs. J. Lipid Res. *55*, 895–904.
42. Leiria, L.O., Wang, C.H., Lynes, M.D., Yang, K., Shamsi, F., Sato, M., Sugimoto, S., Chen, E.Y., Bussberg, V., Narain, N.R., et al. (2019). 12-Lipoxygenase Regulates Cold Adaptation and Glucose Metabolism by Producing the Omega-3 Lipid 12-HEPE from Brown Fat. Cell Metab. *30*, 768–783.e7.
43. Menzies, K.J., Zhang, H., Katsyuba, E., and Auwerx, J. (2016). Protein acetylation in metabolism - metabolites and cofactors. Nat. Rev. Endocrinol. *12*, 43–60.
44. Shahbazian, M.D., and Grunstein, M. (2007). Functions of site-specific histone acetylation and deacetylation. Annu. Rev. Biochem. *76*, 75–100.
45. Morrow, M.R., Batchuluun, B., Wu, J., Ahmadi, E., Leroux, J.M., Mohammadi-Shemirani, P., Desjardins, E.M., Wang, Z., Tsakiridis, E.E., Lavoie, D.C.T., et al. (2022). Inhibition of ATP-citrate lyase improves NASH, liver fibrosis, and dyslipidemia. Cell Metab. *34*, 919–936.e8.
46. Nassir, F., and Ibdah, J.A. (2016). Sirtuins and nonalcoholic fatty liver disease. World J. Gastroenterol. *22*, 10084–10092.
47. Wewer Albrechtsen, N.J., Færch, K., Jensen, T.M., Witte, D.R., Pedersen, J., Mahendran, Y., Jonsson, A.E., Galsgaard, K.D., Winther-Sørensen, M., Torekov, S.S., et al. (2018). Evidence of a liver-alpha cell axis in humans: hepatic insulin resistance attenuates relationship between fasting plasma glucagon and glucagonotropic amino acids. Diabetologia *61*, 671–680.
48. Müller, W.A., Faloona, G.R., and Unger, R.H. (1971). The effect of alanine on glucagon secretion. J. Clin. Invest. *50*, 2215–2218.
49. Kim, J., and Guan, K.L. (2019). mTOR as a central hub of nutrient signalling and cell growth. Nat. Cell Biol. *21*, 63–71.
50. Condon, K.J., and Sabatini, D.M. (2019). Nutrient regulation of mTORC1 at a glance. J. Cell Sci. *132*, jcs222570.
51. Qiu, B., Li, S., Li, M., Wang, S., Mu, G., Chen, K., Wang, M., Zhu, W.G., Wang, W., Wang, J., et al. (2023). KAT8 acetylation-controlled lipolysis affects the invasive and migratory potential of colorectal cancer cells. Cell Death Dis. *14*, 164.
52. Burrell, J.A., and Stephens, J.M. (2021). KAT8, lysine acetyltransferase 8, is required for adipocyte differentiation in vitro. Biochim. Biophys. Acta, Mol. Basis Dis. *1867*, 166103.
53. Puigserver, P., Rhee, J., Donovan, J., Walkey, C.J., Yoon, J.C., Oriente, F., Kitamura, Y., Altomonte, J., Dong, H., Accili, D., and Spiegelman, B.M. (2003). Insulin-regulated hepatic gluconeogenesis through FOXO1-PGC-1alpha interaction. Nature *423*, 550–555.

STAR★METHODS

KEY RESOURCES TABLE

REAGENT or RESOURCE	SOURCE	IDENTIFIER
Antibodies		
Rabbit monoclonal anti-Mof	Abcam	Cat#ab200660; RRID:AB_2891127
Rabbit monoclonal anti-LC3	Abcam	Cat#ab192890; RRID:AB_2827794
Rabbit monoclonal anti-p62	Abcam	Cat#ab109012; RRID:AB_2810880
Rabbit monoclonal anti-Atg7	Abcam	Cat#ab52472; RRID:AB_867756
GAPDH Antibody	Abways	Cat#AB0037; RRID:AB_2891315
Rabbit monoclonal anti-Akt (pan) (C67E7)	Cell Signaling Technology	Cat#4691S; RRID:AB_915783
Rabbit monoclonal anti-Phospho-Akt (Ser473)	Cell Signaling Technology	Cat#4060S; RRID:AB_2315049
Rabbit monoclonal anti-Acetyl-Histone H4 (Lys16)	Cell Signaling Technology	Cat#13534S; RRID:AB_2687581
Rabbit anti-mTOR	Cell Signaling Technology	Cat#2972S; RRID:AB_330978
Rabbit monoclonal anti-Phospho-mTOR (Ser2448)	Cell Signaling Technology	Cat#5536S; RRID:AB_10691552
Rabbit monoclonal anti-Tri-Methyl-Histoe H3 (Lys27)	Cell Signaling Technology	Cat#9733S; RRID:AB_2616029
Rabbit monoclonal anti-Tri-Methyl-Histone H3 (Lys4)	Cell Signaling Technology	Cat#9751S; RRID:AB_2616028
Rabbit monoclonal anti-Acetyl-Histone H3 (Lys27)	Cell Signaling Technology	Cat#8173S; RRID:AB_10949503
Rabbit monoclonal anti-Acetyl-Histone H3 (Lys9)	Cell Signaling Technology	Cat#9649T; RRID:AB_823528
Acetyl-Histone H3 (Lys23) (D6Y7M) Rabbit mAb	Cell Signaling Technology	Cat#14932S; RRID:AB_2798650
Rabbit anti-Acetyl-Histone H2B (Lys20)	Cell Signaling Technology	Cat#2571S; RRID:AB_331546
Rabbit anti-Acetyl-Histone H2B (Lys5)	Cell Signaling Technology	Cat#2574S; RRID:AB_331553
Rabbit anti-Acetyl-Histone H3 (Lys18)	Cell Signaling Technology	Cat#9675T; RRID:AB_331550
Rabbit anti-Acetylated-Lysine	Cell Signaling Technology	Cat#9441S; RRID:AB_331805
Rabbit monoclonal anti-H3	Cell Signaling Technology	Cat#4499S; RRID:AB_10544537
Mouse monoclonal anti-rabbit IgG (Conformation Specific)	Cell Signaling Technology	Cat#3678S; RRID:AB_1549606
Mouse monoclonal anti-ACK (A-11)	Santa Cruz Biotechnology	Cat# sc-28336; RRID:AB_626629
Rabbit polyclonal anti-PPARA	Proteintech	Cat#15540-1-AP; RRID:AB_2252506
PPAR alpha antibody	GeneTex	Cat#GTX101098; RRID:AB_2037654
Mouse monoclonal anti-Phospho-mTOR (Ser2448)	Proteintech	Cat#60004-1-Ig; RRID:AB_2107436
Rabbit polyclonal anti-Cps1	Proteintech	Cat#18703-1-AP; RRID:AB_2084238
Rabbit polyclonal anti-GCK	Proteintech	Cat#19666-1-AP; RRID:AB_10863656
Rabbit polyclonal anti-Histone H4 (Acetyl Lys8)	Immunoway	Cat#YK0012; RRID: AB_2313773
CPT1A Rabbit pAb	Abclonal Technology	Cat#A5307; RRID:AB_2766119
Horseradish Enzyme Labeled Goat anti-rabbit IgG (H + L) (affinity purified)	ZSGB-BIO	Cat#ZB-2301; RRID:AB_2747412
Horseradish Enzyme Labeled Goat anti-mouse IgG (H + L) (affinity purified)	ZSGB-BIO	Cat#ZB-2305; RRID:AB_2747415
Rhodamine (TRITC) - Conjugated Goat anti-Rabbit IgG (H + L)	ZSGB-BIO	Cat#ZF-0316; RRID:AB_2728778
Chemicals, peptides, and recombinant proteins		
MG149	Selleck	S7476; CAS:1243583-85-8
Wy-14643	MedChemExpress	HY-16995; CAS:50892-23-4
palmitic acid	Kunchuang biotechnology	Cat#SYSJ-KJ003
PEG300	Selleck	S6704; CAS: 25322-68-3
Tween80	Selleck	S6702; CAS:9005-65-6

(*Continued on next page*)

Continued

REAGENT or RESOURCE	SOURCE	IDENTIFIER
Glucose anhydrose	MACKLIN	G6172; CAS:50-99-7
Human insulin injection	Wanbang Biopharmaceuticals	Cat#41-1031A
RIPA lysis	Beyotime	Cat#P0013B
Servicebio® 20×Tris-EDTA antigen retrieval solution (pH = 8.0)	Servicebio	Cat#G1206
DAPI Staining Solution	Beyotime	Cat#C1006
Immunol Staining Fix Solution	Beyotime	Cat#P0098
Lipofectamine™ 2000 Transfection Reagent	invitrogen	Cat#18324020
Opti-MEM®I Reduced Serum Medium	Gibco	Cat#2323655
0.25% Trypsin, phenol red	Gibco	Cat#15050057
4-Hydroxytamoxifen	Sigma-Aldrich	CAS:68392-35-8
AML12 specialized medium	Procell	Cat#CM-0602
Critical commercial assays		
9005 SimpleChIP(R) Plus Kit (Magnetic Bead) 4C & RT Reagents	Cell Signaling Technology	Cat#38191S
SimpleChIP® Universal qPCR Master Mix	Cell Signaling Technology	Cat#88989P
Periodic Acid Schiff (PAS) Stain Kit, with Hematoxylin	Solarbio	Cat#G1281
Oil Red O Stain Kit, For Cultured Cells	Solarbio	Cat#G1262
Modified Oil Red O Stain Kit	Solarbio	Cat#G1261
Alanine aminotransferase Assay Kit	Nanjing Jiancheng Bioengineering Institute	Cat#C009-2-1
Aspartate aminotransferase Assay Kit	Nanjing Jiancheng Bioengineering Institute	Cat#C010-2-1
Triglyceride Assay Kit	Nanjing Jiancheng Bioengineering Institute	Cat#A110-1-1
Total cholesterol Assay Kit	Nanjing Jiancheng Bioengineering Institute	Cat#F002-1-1
Liver/Muscle glycogen assay kit	Nanjing Jiancheng Bioengineering Institute	Cat#A043-1-1
DAB Detection Kit (Polymer)	Gene Tech Company Limited	Cat#GK60050
Mouse alanine ELISA Kit	Research Cloud Biology	Cat#KYY-46176M1
E.Z.N.A® Total RNA Kit I	Omega BIO-TEK	Cat#R6834-01
Immobilon Western Chemiluminescent HRP Substrate	Millipore	Cat#WBKLS0500
Evo M-MLV RT Kit with gDNA Clean for qPCR	Accurate Biology	Cat#AG11705
SYBR Green Premix Pro Taq HS qPCR Kit	Accurate Biology	Cat#AG11701
Pierce™ Classic Magnetic IP/Co-IP Kit	Thermo Scientific	Cat#88804
Hematoxylin and Eosin Staining Kit	Beyotime	Cat#C0105
Immobilon®-FL PVDF, 0.45 m, 8.5 cm × 10 m roll	Millipore	Cat#IPFL85R
Deposited data		
Raw data of human NAFLD liver	Suppli MP et al.	GEO: GSE126848
Raw data of livers of Mof knockdown mice	Lei H et al.	GEO: GSE106369
Raw data of mass spectrometry of PPAR alpha	This paper	iProX: PXD046231
Raw data of metabonomics	This paper	MetaboLights: MTBLS8423
Raw data of some western blotting	This paper	Mendeley Data: https://doi.org/10.17632/d6rztmt6gd.1
Experimental models: Cell lines		
Mice: AML12 cells	Procell	Cat#CL-0602; RRID:CVCL_0140
Experimental models: Organisms/strains		
Mouse: C57BL/6J	Beijing Vital River Laboratory Animal Technology Co., Ltd.	N/A
Mouse: Mof flox/flox: B6	Li et al.	N/A
Mouse: B6.129-Gt(ROSA)26Sortm1(cre/ERT2)Tyj/J	The Jackson Laboratory	RRID:IMSR_JAX:008463

(*Continued on next page*)

Continued

REAGENT or RESOURCE	SOURCE	IDENTIFIER
Oligonucleotides		
siRNA targeting sequence: Mof: Sense sequence: CCAUGUGCAGAAGACCUAUTT	GenePharma	N/A
Primer: Mof Forward: ACCTGGGCAAACTCAGCTAC	GenePharma	N/A
Primer: β-actin Forward: CCCAGATCATGTTTGAGACC	GenePharma	N/A
Primer: acot1 Forward: GATGGCCTCAAGGATGTTGT	GenePharma	N/A
Primer: fabp1 Forward: CATCCAGAAAGGGAAGGACA	GenePharma	N/A
Primer: cpt1a Forward: CCAGGCTACAGTGGGACATT	GenePharma	N/A
Primer: hmgcs1 Forward: GGCTGTCAAAACAGTGCTCA	GenePharma	N/A
Primer: tnk2 Forward: ACTGCCACGACCTTTACACC	GenePharma	N/A
ChIP Primer: Tnk2 Forward: GAGAGGAGGAACGGAGCTG	GenePharma	N/A
ChIP primer: Mof 1 Forward: TTCATCGACTAGTTCGCCAC	GenePharma	N/A
ChIP primer: Mof 2 Forward: CCTGAGCGAGAGACGCAAATA	GenePharma	N/A
Software and algorithms		
ImageJ	http://imagej.nih.gov/ij/	RRID:SCR_003070
GraphPad Prism	GraphPad Software. LLC	RRID:SCR_002798
Compound Discoverer3.1(CD) Software	Thermo Fisher	OPTON-31061
Proteome Discoverer2.4	Thermo Fisher	OPTON-31099

RESOURCE AVAILABILITY

Lead contact

Further information and requests for resources and reagents should be directed to and will be fulfilled by the lead contact, Li Chen (chenli3@e-mail.sdu.edu.cn).

Materials availability

This study did not generate new unique reagents.

Data and code availability

- PXD046231data have been deposited at iProX database and are publicly available as of the date of publication. MTBLS8423 data have been deposited at MetaboLights database and are publicly available as of the date of publication. This paper analyzes existing, publicly available data. These accession numbers for the datasets are listed in the key resources table. All data reported in this paper will be shared by the lead contact upon request.
- All original code has been deposited at iProX and MetaboLights, and is publicly available as of the date of publication. DOIs are listed in the key resources table.
- Any additional information required to reanalyze the data reported in this paper is available from the lead contact upon request.

EXPERIMENTAL MODEL AND STUDY PARTICIPANT DETAILS

All animal research complied with the protocols approved by the Animal Care and Use Committee of Shandong University (Issue No. Dwll-2022-135). Mof flox/flox: B6 mice were generated by Xiangzhi Li and B6.129-Gt(ROSA)26Sortm1(cre/ERT2)Tyj/J mice were purchased from The Jackson Laboratory. Eight-week-old male Mof $^{flox/flox}$; ERT-Cre+ mice mice were used for experiments. C57BL/6J mice were purchased from the Beijing Vital River Laboratory Animal Technology Co., Ltd. and eight-week-old male C57BL/6J mice were used for analysis. To establish DIO models, four-week-old male C57BL/6J mice were given 12 weeks of high-fat diet. All mice were housed in a specific pathogen-free (SPF) animal room with a 12-h light/12-h dark cycle and free access to food and water. Mice hepatic cell line AML 12 was obtained from Procell. Ltd and cultured in a specialized medium.

METHOD DETAILS

Mice experiments

In Mof $^{flox/flox}$; ERT-Cre+ mice, 4-OHT (CAS:68392-35-8, Sigma-Aldrich, USA) was administrated by intraperitoneal injection for continuous 4 days. Then after a 7 days chase, other experiments were conducted. WT mice were given a chow diet and DIO mice were given 60% high-fat diet. These mice were randomly divided into 2 groups. From 8 weeks, one group was given 1 mg/kg mg149 (CAS:1243583-85-8, Sellck, China) dissolved in DMSO, Tween 80 (CAS:9005-65-6, Sellck), and PEG 300 (CAS: 25322-68-3, Selleck), intraperitoneally every other day, while the other was given DMSO solvent as control.

IPGTT was carried out with the glucose anhydrose (CAS:50-99-7, MACKLIN, USA) dosage of 1.5 g/kg body weight after 12–14 h fasting. IPITT was executed with the human insulin (Cat#41-1031A, Wanbang Biopharmaceuticals, China) of 0.75 U/kg body weight after 6–8 h fasting. Tail vein blood glucose was measured by Accu-Chek Performa.

After mice being sacrificed under anesthesia, serums were stored at −80°C for future usage. Part of the livers were fixed in 4% paraformaldehyde, embedded in paraffin, and sectioned into slides. These slides were used for HE, PAS, IHC, and IF staining. Part of the livers were sectioned as frozen slides, used for Oil-O staining. Part of the livers were frozen in liquid nitrogen for 15 min, and then utilized for metabonomics tests. The remaining tissues were used for protein extraction and Western blotting.

Cell culture and treatment

AML 12 cell line (Cat#CL-0602, Procell, China) was cultured in a specialized medium (Cat#CM-0602, Procell). Mof activity inhibition was achieved via 35 nM mg149 (CAS:1243583-85-8, Sellck, China) administration for 1 day. When necessary, 0.3 mM PA (Cat#SYSJ-KJ003, Kunchuang biotechnology, China) or 10 μM PPARα agonist wy-14643 (CAS:50892-23-4, MedChemExpress, China) was added to the specialized medium for 24 h. Cell lines were sub-cultured by 0.25% Trypsin-EDTA (Cat#15050057, Gibco, USA). Sequences of siRNAs (Sense sequence: CCAUGUGCAGAAGACCUAUTT) targeting Mof were designed and synthesized by GenePharma (Shanghai, China). For transfection, AML 12 cells were transfected with 160 pmol siRNA using Lipofectamine 2000 Transfection Reagent (Cat#18324020, Invitrogen, USA) in Opti-MEMI Reduced Serum Medium (Cat#2323655, Gibco) according to manufacturer's instructions. Cells were harvested 48 h later for RNA or 72 h for protein.

HE, PAS, and Oil-O staining

HE staining was conducted according to the standard protocol via Hematoxylin and Eosin Staining Kit (Cat#C0105, Beyotime, China). Basically, after being dewaxed in xylene and ethanol, paraffin-embedded slides were stained in hematoxylin for 2 min and in eosin for 1 min. PAS staining was performed according to the instruction of the PAS staining kit (Cat#G1281, Solarbio, China). Oil-O staining of frozen slides and cultured cells were conducted using the Oil-O kit (Cat#G1261, Solarbio) and the Oil-O kit specialized for cultured cells(Cat#G1262, Solarbio). The pictures were taken by CellSens Standard. The quantification of Oil-O staining results was performed by assessing the proportion of positively stained area in relation to the overall valid areas using ImageJ software.

IHC and IF staining

To perform IHC staining, after deparaffinating, antigen retrieval was achieved by citrate buffer (pH = 8.0) (Cat#G1206, Servicebio). Endogenous catalase and unspecific binding site were blocked by 3% H_2O_2 provided by the kit (Cat#GK60050, Gene Tech Company Limited, China) and goat serum respectively. The primary antibody (Mof 1:100, Cat#ab200660, Abcam, USA; Phospho-mTOR (Ser2448) 1:100, Cat#5536S, CST, USA; Akt (pan) 1:100, Cat#4691S, CST; and Phospho-Akt (Ser473) 1:100, Cat#4060S, CST) was incubated overnight at 4°C. On the following day, the secondary antibody staining and DAB staining were performed according to the protocol provided by the DAB Detection Kit.

For IF staining, after antigen retrieval and blocking unspecific sites, anti-H4K16ac (1:100, Cat#13534S, CST) was incubated overnight at 4°C. On the following day, fluorophore-conjugated secondary antibodies (1:200, Cat#ZF-0316, ZSGB-BIO, China) were applied at 37°C for 1 h. After DAPI (Cat#C1006, Beyotime) staining for 5 min at room temperature, pictures were taken by CellSens Standard.

Western blotting

Briefly, the protein was extracted via lysis buffer and separated by SDS-PAGE. Then we transferred protein onto PVDF membranes (Cat#IPFL85R, Millipore, USA). After being blocked, membranes were incubated with primary antibodies at 4°C overnight. The primary antibodies used were as following: GAPDH 1:1000, Cat#AB0037, Abways, China; Cps1 1:1000, Cat#18703-1-AP, Proteintech, China; Mof 1:1000, Cat#ab200660, Abcam; H4K16ac 1:1000, Cat#13534S, CST; GCK 1:1000, Cat#19666-1-AP, Proteintech; PPARα 1:1000, Cat#15540-1-AP, Proteintech; LC3 1:1000, Cat#ab192890, Abcam; p62 1:1000, Cat#ab109012, Abcam; Atg7 1:1000, Cat#ab52472, Abcam; H4K8ac 1:1000, Cat#YK0012, Immunoway, USA; Phospho-mTOR (Ser2448) 1:1000, Cat#5536S, CSTl mTOR 1:1000, Cat#2972S, CST; H3 1:1000, Cat#9733S, CST; Acetyl lysine 1:1000, Cat#9441S, CST; Tnk2 1:500, Cat# sc-28336, Santa Cruz Biotechnology, USA; Akt (pan) 1:1000, Cat#4691S, CST; Phospho-Akt (Ser473) 1:1000, Cat#4060S, CST; Cpt1a 1:500, Cat#A5307, Abclonal Technology; H3K27ac 1:1000, Cat#8173S, CST; H3K9ac 1:1000, Cat#9649T, CST; H3K23ac 1:1000, Cat#14932S, CST; H2BK20ac 1:1000, Cat#2571S, CST; H2BK5ac 1:1000, Cat#2574S, CST; and H3K18ac 1:1000, Cat#9675T, CST.

The next day, secondary antibodies conjugated with horseradish peroxidase (1:10000, Cat#ZB-2301 and Cat#ZB-2305, ZSGB-BIO) were incubated for 2 h at room temperature. The immune complexes were detected with an enhanced chemiluminescence kit (Cat#WBKLS0500, Millipore).

Enzyme-linked immunosorbent assay (ELISA)

For the measurement of serum and intra-hepatic alanine levels, ELISA tests were carried out with a mouse alanine kit (Cat#KYY-46176M1, Research Cloud Biology, China) in accordance with the protocols provided.

ALT, AST, TG, cholesterol, and glycogen measurements

Biochemical items testing including ALT (Cat#C009-2-1, Nanjing Jiancheng Bioengineering Institute, China), AST (Cat#C010-2-1, Nanjing Jiancheng Bioengineering Institute), TG (Cat#A110-1-1, Nanjing Jiancheng Bioengineering Institute), cholesterol (Cat#F002-1-1, Nanjing Jiancheng Bioengineering Institute), and glycogen (Cat#A043-1-1, Nanjing Jiancheng Bioengineering Institute) were all performed via kits purchased from Nanjing Jiancheng Bioengineering Institute. ALT testings were performed with the kit based on the reaction between ALT and alanine/α-ketoglutaric acid. AST kits were based on the interactions between AST and aspartic acid. ALT and AST concentrations were measured according to the absorption at 510 nm wavelength. TG and cholesterol kits were applied with the GPO-PAP mechanism. Serum TG and cholesterol levels were calculated according to the absorption at 500 nm and 510 nm wavelength, respectively. Intra-hepatic lipids were extracted via ethanol and the levels were corrected according to the liver weight used for analysis. Glycogen testings were based on the reaction between glycogen and concentrated sulfuric acid and the glycogen levels were measured at 620 nm wavelength and corrected according to the liver weight used for analysis.

RNA extraction and qRT-PCR

RNA extraction was conducted according to E.Z.N.A Total RNA Kit I (Cat#R6834-01, Omega BIO-TEK, USA). cDNA synthesis was conducted using Evo M-MLV RT Kit with gDNA Clean for qPCR (Cat#AG11705, Accurate Biology, China) and q-PCR were performed using SYBR Green Premix Pro Taq HS qPCR Kit (Cat#AG11701, Accurate Biology). Primers were designed with Primer 6.0 software and synthesized by GenePharma (Shanghai, China). PCR was programmed as follows: 5 min at 94°C, 40 cycles of 94°C for 30 s, 60°C for 30 s, and 72°C for 40 s, and a 5 s incubation at 65°C. Primers used in this manuscript were as followings: *β-actin* F: CCCAGATCATGTTTGAGACC; *Acot1* F: GATGGCCTCAAGGATGTTGT; *Fabp1* F: CATCCAGAAAGGGAAGGACA; *Mof* F: ACCTGGGCAAACTCAGCTAC; *Hmgcs* F : GGCTGT CAAAACAGTGCTCA; *Tnk2* F: ACTGCCACGACCTTTACACC; *Cpt1a* F: CCAGGCTACAGTGGGACATT.

Co-IP

Co-IP was conducted according to the protocol provided by PierceTM Classic Magnetic IP/Co-IP Kit (Cat#88804, Thermo Scientific). To detect the interaction between PPARα and Mof and to detect the lysine acetylation on PPARα, primary antibodies used were Mof (Cat#ab200660, Abcam), PPARα (Cat#15540-1-AP, Proteintech), and Ac-lysine (Cat#9441, CST). On the second day, conformation-specific secondary mouse anti-rabbit IgG antibodies (1:1000, Cat#3678S, CST) were used. To detect the acetylated lysine sites on PPARα, immunoprecipitation based on PPARα antibody (Cat#GTX101098, GeneTex, China) were performed and the product was used for mass spectrometry.

ChIP and ChIP-qPCR

ChIP was performed according to the instruction provided by 9005 SimpleChIP(R) Plus Kit (Magnetic Bead) (Cat#38191S). Briefly, the AML 12 cells or minced tissues were cross-linked by 37% formaldehyde and glycine. Then nuclei preparation and chromatin digestion were conducted by micrococcal nuclease and sonication. Chromatin immunoprecipitation were performed using anti-H4K16ac (Cat#13534S, CST), anti-H3K27ac (Cat#8173S, CST), anti-H3K4me3 (Cat#9751S, CST), and anti-H3K27me3 (Cat#9733S, CST). Then, chromatin was washed from Antibody/Protein G Magnetic Beads and purified using spin columns. q-PCR was performed as the protocol given by SimpleChIP Universal qPCR Master Mix (Cat#88989, CST). The ChIP primer sequences were as followings: Tnk2: Forward: GAGAGGAGGAACGGAGCTG; Mof1: Forward: TTCATCGACTAGTTCGCCAC; Mof2: CCTGAGCGAGAGACGCAAATA. Percentage of input was calculated as $2\% \times 2^{(C[T]\ 2\%Input\ Sample\ -\ C[T]\ IP\ Sample)}$.

Mass spectrometry (MS) and raw data analysis

The stained protein bands were cut into 1 mm^3 pieces, detained with acetonitrile (ACN) and vacuum dried. Proteins on the gels were treated with 10 mM DTT for 1 h at 37°C and subsequently alkylated with 55 mM iodoacetamide for 30 min in the dark. Then ACN was added again to dehydrate and deionized water added for cleaning. Next, ammonium bicarbonate was added for 10 min, then trypsin was added. After the enzyme solution is completely absorbed by the micelles, the gel was incubate at 37°C overnight; the next day, we add ACN, collect the hydrolysis supernatant by centrifugation, and add 0.1% FA to the remaining colloidal particles. The solution was used for analysis.

Nanoflow LC-MS/MS analysis of tryptic peptides was conducted on a quadrupole Orbitrap mass spectrometer (Orbitrap Exploris 480, Thermo Fisher Scientific, Bremen, Germany) coupled to an EASY nLC 1200 ultra-high pressure system (Thermo Fisher Scientific) via a nano-electrospray ion source. All raw files were analyzed using the Proteome Discoverer suite (version 2.4, Thermo Fisher Scientific). MS2 spectra were searched against the UniProtKB human proteome database containing both Swiss-Prot and TrEMBL human reference protein

sequences (20,373 target sequences downloaded on 17 March 2022). The Sequest HT search engine was used, and parameters were specified as follows: fully tryptic specificity, maximum of three missed cleavages, minimum peptide length of 6, fixed carbamidomethylation of cysteine residues (+57.02146Da) and Acetylation of lysine(42.01Da), variable modifications for oxidation of methionine residues (+15.99492Da), precursor mass tolerance of 15 ppm and a fragment mass tolerance of 0.02Da for MS2 spectra collected in the Orbitrap. Percolator was used to filter peptide spectral matches and peptides to a false discovery rate (FDR) of less than 1%. After spectral assignment, peptides were assembled into proteins and were further filtered based on the combined probabilities of their constituent peptides to a final FDR of 1%. As default, the top matching protein or 'master protein' was the protein with the largest number of unique peptides and with the smallest value in the percent peptide coverage (that is, the longest protein). Only unique and razor (that is, parsimonious) peptides were considered for quantification. The original raw data have been uploaded to iProX database with the identifier PXD046231.

Transcriptomics data analysis

Transcriptional data of human liver tissues (normal weight, obese, NAFL, NASH) were downloaded from GSE126848. Transcriptional data of Mof-deficient livers (Mof $^{flox/flox}$ and Mof $^{flox/flox}$; Mx1-Cre) were downloaded from GSE106369. Because the data from one of the three Mof $^{flox/flox}$; Mx1-Cre was similar to Mof$^{f\ lox/flox}$ mice, the raw data from GSE106369 was re-analyzed as three Mof $^{flox/flox}$ mice versus two Mof$^{f\ lox/flox}$; Mx1-Cre mice, fold-change $\geq$2 was adopted as the standard for differentially expressed genes. To clarify the biological functions and involved signaling pathways, we annotated each gene based on the GO and KEGG database. Enrichment calculations were performed using Fisher's exact test.

Metabonomics and raw data analysis

To extract metabolites from liver samples, 1 mL cold extraction solvent methanol/acetonitrile/H_2O (2:2:1) was added to the 80 mg sample, and adequately vortexed. The lysate was homogenized by MP homogenizer and sonicated at 4°C then centrifuged. The supernatant was dried in a vacuum centrifuge at 4°C. For LC-MS analysis, the samples were re-dissolved in 100 μL acetonitrile/water (1:1) solvent. For untargeted metabolomics of polar metabolites, extracts were analyzed using a quadrupole time-of-flight mass spectrometer (Sciex TripleTOF 6600) coupled to hydrophilic interaction chromatography via electrospray ionization in Shanghai Applied Protein Technology Co., Ltd. The mass spectrometer was operated in both negative ion and positive ionization modes. Compound identification of metabolites by MS/MS spectra with an in-house database established with available authentic standards. The original raw data have been uploaded to MetaboLights with the identifier MTBLS8423. After normalized to total peak intensity, the processed data were uploaded before importing into SIMCA-P (version 14.1, Umetrics, Umea, Sweden), where it was subjected to multivariate data analysis, including Pareto-scaled principal component analysis (PCA) and orthogonal partial least-squares discriminant analysis (OPLS-DA). The 7-fold cross-validation and response permutation testing were used to evaluate the robustness of the model. The variable importance in the projection (VIP) value of each variable in the OPLS-DA model was calculated to indicate its contribution to the classification. Significance was determined using an unpaired Student's *t* test. VIP value > 1 and $p < 0.05$ was considered statistically significant. For KEGG annotation, metabolites were blasted against the online Kyoto Encyclopedia of Genes and Genomes (KEGG) database to retrieve their COs and were subsequently mapped to pathways in KEGG. KEGG pathway enrichment analyses were applied based on Fisher' exact test. Pathways with p values under a threshold of 0.05 were considered as significantly changed pathways.

QUANTIFICATION AND STATISTICAL ANALYSIS

Graph data were presented as mean ± SEM and analyzed with GraphPad Software. The sample size for the animal experiments was determined based on the literature and our previous experience with similar experiments. Nanoflow LC-MS/MS analysis of tryptic peptides was conducted on a quadrupole Orbitrap mass spectrometer (Orbitrap Exploris 480, Thermo Fisher Scientific, Bremen, Germany) coupled to an EASY nLC 1200 ultra-high pressure system (Thermo Fisher Scientific) via a nano-electrospray ion source. Raw files were analyzed using the Proteome Discoverer suite (version 2.4, Thermo Fisher Scientific). The raw data from GSE106369 was re-analyzed where fold-change $\geq$2 was adopted as the standard for differentially expressed genes. For the analysis of metabonomics raw data, the variable importance in the projection (VIP) value of each variable in the OPLS-DA model was calculated to indicate its contribution to the classification. Significance was determined using an unpaired Student's *t* test. VIP value > 1 and $p < 0.05$ was considered statistically significant. Enrichment calculations of KEGG were performed using Fisher's exact test. p value < 0.05 was taken to indicate a statistically significant difference. *p stands for < 0.05, **p for < 0.01, and ***p for < 0.001. Statistical details are described in figure legends and supplementary figure legends, including the statistical tests used, exact value of n, what n represents, and dispersion and precision measures.